

# STATUS OF DELAYED-NEUTRON PRECURSOR DATA: HALF-LIVES AND NEUTRON EMISSION PROBABILITIES

Bernd Pfeiffer<sup>1</sup> and Karl-Ludwig Kratz  
*Institut für Kernchemie, Universität Mainz, Germany*

Peter Möller  
*Theoretical Division, Los Alamos National Laboratory, Los Alamos, NM 87545*

ABSTRACT: – We present in this paper a compilation of the present status of experimental delayed-neutron precursor data; i.e.  $\beta$ -decay half-lives ( $T_{1/2}$ ) and neutron emission probabilities ( $P_n$ ) in the fission-product region ( $27 \leq Z \leq 57$ ). These data are compared to two model predictions of substantially different sophistication: (i) an update of the empirical Kratz–Herrmann formula (KHF), and (ii) a unified macroscopic-microscopic model within the quasi-particle random-phase approximation (QRPA). Both models are also used to calculate so far unknown  $T_{1/2}$  and  $P_n$  values up to  $Z = 63$ . A number of possible refinements in the microscopic calculations are suggested to further improve the nuclear-physics foundation of these data for reactor and astrophysical applications.

## INTRODUCTION

Half-lives ( $T_{1/2}$ ) and delayed-neutron emission probabilities ( $P_n$ ) are among the easiest measurable gross  $\beta$ -decay properties of neutron-rich nuclei far from stability. They are not only of importance for reactor applications, but also in the context of studying nuclear-structure features and astrophysical scenarios. Therefore, most of our recent experiments performed at international facilities such as CERN-ISOLDE, GANIL-LISE and GSI-FRS were primarily motivated by our current work on r-process nucleosynthesis. However, it is a pleasure for us to recognize that these data still today may be of interest for applications in reactor physics, a field which we practically left shortly after the "Specialists' Meeting on Delayed Neutrons" held at Birmingham in 1986.

Our motivation to put together this new compilation of  $\beta$ -decay half-lives and  $\beta$ -delayed neutron-emission came from recent discussions with T.R. England and W.B. Wilson from LANL about our activities in compiling and steadily updating experimental delayed-neutron data as well as various theoretical model predictions (Pfeiffer *et al.*, 2000). They pointed out to us, that their recent summation calculations of aggregate fission-product delayed-neutron production using basic nuclear data from the early 1990's (Brady, 1989; Brady and England, 1989, Rudstam 1993) show, in general, that a greater fraction of delayed neutrons is emitted at earlier times following fission than measured. As a consequence, the reactor response to a reference reactivity change is enhanced compared to that calculated with pulse functions derived from measurements (Wilson and England, 2000). Therefore, the use of updated  $\beta_n$  and  $T_{1/2}$  values is expected to improve the physics foundation of the basic input data used and to increase the accuracy of aggregate results obtained in summation calculations.

Since the tabulation of Brady (1989) and Rudstam (1993), about 40 new  $\beta_n$  values have been measured in the fission-product region ( $27 \leq Z \leq 57$ ), a number of delayed-neutron

---

<sup>1</sup>E-mail address: Bernd.Pfeiffer@uni-mainz.de

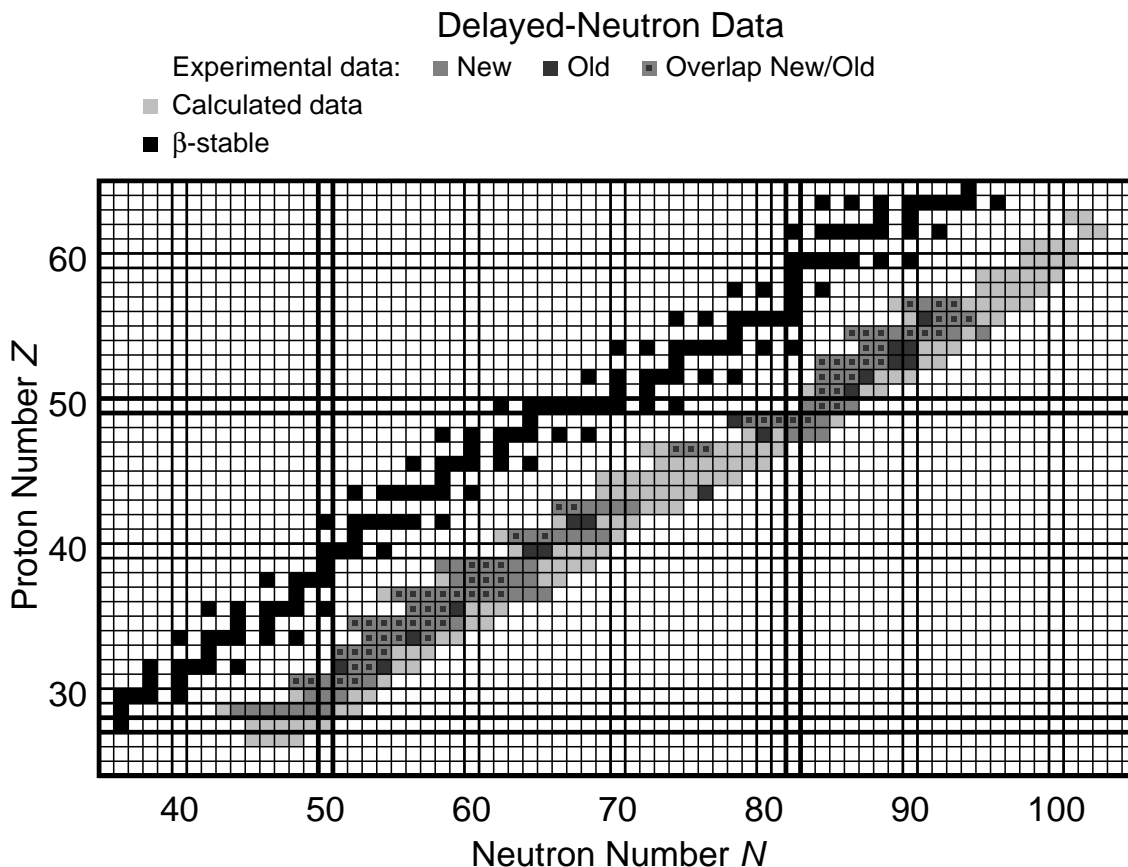


Figure 1: Chart illustrating the data available in the fission-product region. The new data evaluation represents a significant extension of measured  $P_n$  values. Some data in the old data set are not present in the new data set.

branching ratios have also been determined with higher precision, and a similar number of ground-state and isomer decay half-lives of new delayed-neutron precursors have been obtained. These data are contained in our compilation (Table 1), and are compared with two of our model predictions: (i) an update of the empirical Kratz-Herrmann formula (KHF) for  $\beta$ -delayed neutron emission probabilities  $P_n$  and  $\beta$ -decay half-lives  $T_{1/2}$  (Kratz and Herrmann, 1973; Pfeiffer, 2000), and an improved version of the macroscopic-microscopic QRPA model (Möller and Randrup, 1990) which can be used to calculate a large number of nuclear properties consistently (Möller *et al.*, 1997). These two models, with quite different nuclear-structure basis, are also used to predict so far unknown  $T_{1/2}$  and  $P_n$  values in the fission-product region (see Table 1).

#### EXPERIMENTAL DATA

Most of the new  $\beta$ -decay half-lives of the very neutron-rich delayed-neutron precursor isotopes included in Table 1 have been determined from growth-and-decay curves of neutrons detected with standard neutron-longcounter set-ups. As an example, the presently

Table 1: Experimental  $\beta$ -decay half-lives  $T_{1/2}$  and  $\beta$ -delayed neutron-emission probabilities  $P_n$  compared to three calculations.

Isotope	$T_{1/2}$ (ms)					$P_n$ (%)				
	Exp.		KHF	QRPA-1	QRPA-2	Exp.		KHF	QRPA-1	QRPA-2
$^{66}_{27}\text{Co}$	180	10	432	260	260			0.013	0.000	0.000
$^{67}_{27}\text{Co}$	425	20	400	76	120			1.132	0.156	0.061
$^{68}_{27}\text{Co}$	230	30	168	72	82			2.395	0.812	0.768
$^{68\text{m}}_{27}\text{Co}$	1600	300								
$^{69}_{27}\text{Co}$	216	9	238	64	99			6.585	1.250	0.905
$^{70}_{27}\text{Co}$	120	30	101	43	60			7.469	3.213	2.154
$^{70\text{m}}_{27}\text{Co}$	500	180								
$^{71}_{27}\text{Co}$	270	50	109	42	60			16.650	3.468	2.666
$^{72}_{27}\text{Co}$	100	50	58	29	52			13.350	5.810	3.721
$^{73}_{27}\text{Co}$			63	27	33			28.230	6.153	3.441
$^{74}_{27}\text{Co}$			35	17	25			20.700	9.858	5.962
$^{75}_{27}\text{Co}$			34	15	20			37.920	8.027	7.407
$^{76}_{27}\text{Co}$			21	11	17			29.690	11.034	24.677
$^{77}_{27}\text{Co}$			20	10	15			52.810	39.341	78.079
$^{72}_{28}\text{Ni}$	1570	50	859	8141	8141			0.000	0.000	0.000
$^{73}_{28}\text{Ni}$	840	30	251	2358	2025			0.097	0.193	0.226
$^{74}_{28}\text{Ni}$	500	200	271	2056	1508			0.632	3.098	2.853
$^{75}_{28}\text{Ni}$	700	400	114	890	696			1.477	8.967	9.127
$^{76}_{28}\text{Ni}$	440	400	126	920	593			4.108	26.207	23.952
$^{77}_{28}\text{Ni}$			61	372	323			4.859	36.401	38.724
$^{78}_{28}\text{Ni}$			66	332	326			10.810	40.662	55.747
$^{79}_{28}\text{Ni}$			26	126	48			14.330	92.135	81.490
$^{73}_{29}\text{Cu}$	3900	300	1936	4092	2726	0.029	6	0.045	0.018	0.011
$^{74}_{29}\text{Cu}$	1594	10	393	1308	957	0.075	16	0.117	0.306	0.158
$^{75}_{29}\text{Cu}$	1224	3	458	1345	844	2.6	5	3.982	5.840	2.946
$^{76}_{29}\text{Cu}$	641	6	153	657	428	2.4	5	2.880	6.706	3.252
$^{76\text{m}}_{29}\text{Cu}$	1270	300								
$^{77}_{29}\text{Cu}$	469	8	155	764	405	15	$^{+10}_{-5}$	11.730	26.228	12.380
$^{78}_{29}\text{Cu}$	342	11	77	351	268	15	$^{+10}_{-5}$	11.990	37.899	13.865
$^{79}_{29}\text{Cu}$	188	25	76	358	212	55	17	21.830	33.698	27.861
$^{80}_{29}\text{Cu}$			26	97	149			22.530	62.342	76.800
$^{81}_{29}\text{Cu}$			28	90	170			72.270	99.985	100.000
$^{82}_{29}\text{Cu}$			18	40	40			61.680	98.931	98.931
$^{77}_{30}\text{Zn}$	2080	50	689	8888	8888			0.000	0.000	0.000
$^{77\text{m}}_{30}\text{Zn}$	1050	100								
$^{78}_{30}\text{Zn}$	1470	150	419	5022	15694			0.001	0.027	0.000
$^{79}_{30}\text{Zn}$	995	19	225	3925	3098	1.3	4	0.238	0.958	0.364

Table 1: Continued

Isotope	$T_{1/2}$ (ms)					$P_n$ (%)				
	Exp.		KHF	QRPA-1	QRPA-2	Exp.		KHF	QRPA-1	QRPA-2
$^{80}_{30}\text{Zn}$	545	16	255	3025	2033	1.0	5	0.668	10.889	9.980
$^{81}_{30}\text{Zn}$	290	50	64	646	2401	7.5	30	2.343	21.952	60.505
$^{82}_{30}\text{Zn}$			52	211	734			17.170	35.281	99.972
$^{83}_{30}\text{Zn}$			43	22	818			23.300	9.816	99.982
$^{84}_{30}\text{Zn}$			43	65	387			25.480	33.273	100.000
$^{79}_{31}\text{Ga}$	2847	3	999	3463	2062	0.080	14	0.119	0.110	0.055
$^{80}_{31}\text{Ga}$	1697	11	301	1575	2413	0.85	6	0.468	0.865	0.626
$^{81}_{31}\text{Ga}$	1217	5	404	1684	1852	12.1	4	3.776	6.666	6.956
$^{82}_{31}\text{Ga}$	599	2	96	496	1817	22.3	22	5.548	13.248	24.235
$^{83}_{31}\text{Ga}$	308	1	82	202	891	38.7	98	33.790	76.668	98.359
$^{84}_{31}\text{Ga}$	85	10	56	22	1644	70	15	28.150	15.387	99.982
$^{85}_{31}\text{Ga}$			48	71	686			60.390	99.953	100.000
$^{86}_{31}\text{Ga}$			29	22	409			42.400	67.188	99.994
$^{87}_{31}\text{Ga}$			29	24	118			73.540	99.930	100.000
$^{83}_{32}\text{Ge}$	1850	60	249	2115	70415			0.019	0.109	2.198
$^{84}_{32}\text{Ge}$	954	14	207	1046	16208	10.2	9	1.747	8.565	76.205
$^{85}_{32}\text{Ge}$	540	50	131	40	9900	14	3	4.297	1.615	99.088
$^{86}_{32}\text{Ge}$			95	184	2168			6.044	6.647	65.566
$^{87}_{32}\text{Ge}$			64	44	1356			11.430	5.104	93.931
$^{88}_{32}\text{Ge}$			66	46	256			17.480	5.595	65.740
$^{89}_{32}\text{Ge}$			39	17	20			19.090	15.824	9.194
$^{84}_{33}\text{As}$	4020	30	392	3548	16635	0.18	10	0.026	0.302	0.373
$^{84m}_{33}\text{As}$	650	150								
$^{85}_{33}\text{As}$	2022	9	280	2485	9431	55	14	7.935	17.599	48.990
$^{86}_{33}\text{As}$	945	8	191	187	5023	26	7	9.290	10.392	92.592
$^{87}_{33}\text{As}$	560	110	137	269	2458	17.5	25	17.890	32.629	100.000
$^{88}_{33}\text{As}$			112	61	2263			23.060	35.870	99.924
$^{89}_{33}\text{As}$			59	66	374			29.690	90.576	100.000
$^{90}_{33}\text{As}$			43	23	21			30.830	41.952	22.786
$^{91}_{33}\text{As}$			44	36	73			58.130	99.784	100.000
$^{92}_{33}\text{As}$			27	36	36			40.550	90.468	90.468
$^{86}_{34}\text{Se}$	15300	900	1063	12602	12602			0.000	0.000	0.000
$^{87}_{34}\text{Se}$	5500	140	657	677	1885875	0.36	8	0.020	0.012	3.109
$^{88}_{34}\text{Se}$	1520	30	327	403	12312	0.67	30	0.193	0.231	0.986
$^{89}_{34}\text{Se}$	410	40	232	114	9050	7.8	25	1.198	0.519	9.187
$^{90}_{34}\text{Se}$			161	134	1127			2.991	0.859	0.923
$^{91}_{34}\text{Se}$	270	50	104	34	40	21	10	8.353	1.524	3.045

Table 1: Continued

Isotope	$T_{1/2}$ (ms)					$P_n$ (%)				
	Exp.		KHF	QRPA-1	QRPA-2	Exp.		KHF	QRPA-1	QRPA-2
$^{92}_{34}\text{Se}$			93	59	164			11.770	2.187	1.312
$^{93}_{34}\text{Se}$			62	87	24			10.910	24.270	9.342
$^{94}_{34}\text{Se}$			59	52	43			13.830	19.996	1.712
$^{87}_{35}\text{Br}$	55600	150	1059	12315	37254	2.52	7	0.146	0.277	1.129
$^{88}_{35}\text{Br}$	16360	70	685	1386	104991	6.55	18	0.466	0.194	28.599
$^{89}_{35}\text{Br}$	4400	30	429	203	10758	13.7	4	2.445	0.255	41.746
$^{90}_{35}\text{Br}$	1910	10	283	108	17328	24.9	10	5.622	1.818	99.800
$^{91}_{35}\text{Br}$	541	5	172	55	762	31.3	60	12.050	3.319	73.365
$^{92}_{35}\text{Br}$	343	15	111	36	54	33.7	12	19.710	13.032	8.458
$^{93}_{35}\text{Br}$	102	10	97	46	221	65	8	33.730	21.507	100.000
$^{94}_{35}\text{Br}$	70	20	69	133	34	68	16	29.120	48.680	14.221
$^{95}_{35}\text{Br}$			66	77	57			34.000	70.822	100.000
$^{96}_{35}\text{Br}$			42	42	19			27.600	52.064	33.573
$^{97}_{35}\text{Br}$			40	49	49			46.800	95.558	95.558
$^{91}_{36}\text{Kr}$	8570	40	1213	500	500			0.000	0.000	0.000
$^{92}_{36}\text{Kr}$	1840	8	560	396	1934	0.033	3	0.010	0.012	0.051
$^{93}_{36}\text{Kr}$	1286	10	282	516	78	1.95	11	0.799	1.079	0.012
$^{94}_{36}\text{Kr}$	200	10	239	548	559	5.7	22	2.084	0.953	0.090
$^{95}_{36}\text{Kr}$	780	30	150	373	61			4.144	4.942	0.725
$^{96}_{36}\text{Kr}$			161	196	118			6.118	5.945	0.322
$^{97}_{36}\text{Kr}$			111	81	32			6.214	6.104	2.485
$^{98}_{36}\text{Kr}$			87	106	38			7.633	9.143	1.088
$^{99}_{36}\text{Kr}$			52	72	72			11.600	33.873	33.873
$^{100}_{36}\text{Kr}$			51	48	48			16.610	25.386	25.386
$^{91}_{37}\text{Rb}$	58400	400	2363	19066	408587			0.000	0.000	0.001
$^{92}_{37}\text{Rb}$	4492	20	1265	279	723153	0.011	1	0.015	0.001	4.142
$^{93}_{37}\text{Rb}$	5840	20	661	184	5735	1.44	10	0.830	0.116	5.259
$^{94}_{37}\text{Rb}$	2702	5	285	158	119	9.1	11	2.755	1.414	1.628
$^{95}_{37}\text{Rb}$	377.5	8	221	78	386	8.73	31	10.740	2.989	37.932
$^{96}_{37}\text{Rb}$	203	3	135	71	57	13.3	7	13.220	10.634	10.546
$^{97}_{37}\text{Rb}$	169.9	7	126	46	46	26.0	19	20.530	12.529	12.529
$^{98}_{37}\text{Rb}$	96	3	103	52	52	14.6	18	15.070	16.598	16.598
$^{98\text{m}}_{37}\text{Rb}$	114	5								
$^{99}_{37}\text{Rb}$	50.3	7	86	43	43	17.3	25	29.310	26.876	26.876
$^{100}_{37}\text{Rb}$	51	8	63	38	38	12	7	15.900	26.153	26.153
$^{100\text{m}}_{37}\text{Rb}$										
$^{101}_{37}\text{Rb}$	32	4	70	39	39	25	5	36.800	33.729	33.729

Table 1: Continued

Isotope	$T_{1/2}$ (ms)					$P_n$ (%)				
	Exp.		KHF	QRPA-1	QRPA-2	Exp.		KHF	QRPA-1	QRPA-2
$^{102}_{37}\text{Rb}$	37	5	36	13	13	18	8	25.270	20.312	20.312
$^{103}_{37}\text{Rb}$			39	17	17			48.740	52.410	52.410
$^{104}_{37}\text{Rb}$			27	13	13			37.980	58.332	58.332
$^{105}_{37}\text{Rb}$			28	12	12			55.730	73.481	73.481
$^{96}_{38}\text{Sr}$	1070	10	854	1079	817			0.000	0.000	0.000
$^{97}_{38}\text{Sr}$	429	5	556	1179	119	0.02	1	0.109	0.232	0.001
$^{98}_{38}\text{Sr}$	653	2	626	724	724	0.40	17	0.161	0.380	0.380
$^{99}_{38}\text{Sr}$	269	1	373	359	359	0.25	10	0.504	0.227	0.227
$^{100}_{38}\text{Sr}$	202	3	289	495	495	1.11	34	0.168	0.437	0.437
$^{101}_{38}\text{Sr}$	118	3	171	375	375	2.75	35	2.346	3.944	3.944
$^{102}_{38}\text{Sr}$	69	6	120	142	142	5.5	15	1.450	3.026	3.026
$^{103}_{38}\text{Sr}$			79	35	35			9.952	2.153	2.153
$^{104}_{38}\text{Sr}$			68	79	79			8.340	7.477	7.477
$^{105}_{38}\text{Sr}$			61	49	49			10.420	14.502	14.502
$^{96}_{39}\text{Y}$	5340	50	3009	1439	1413			0.000	0.000	0.000
$^{96\text{m}}_{39}\text{Y}$	9600	200								
$^{97}_{39}\text{Y}$	3750	30	1148	288	5030	0.045	20	0.066	0.014	0.015
$^{97\text{m}1}_{39}\text{Y}$	1170	30				$\leq 0.08$				
$^{97\text{m}2}_{39}\text{Y}$	142	8								
$^{98}_{39}\text{Y}$	548	2	696	305	302	0.295	33	1.469	0.375	1.253
$^{98\text{m}}_{39}\text{Y}$	2000	200				3.4	10			
$^{99}_{39}\text{Y}$	1470	7	602	167	167	2.2	5	3.385	0.492	0.492
$^{100}_{39}\text{Y}$	735	7	496	318	318	1.16	32	0.951	0.309	0.309
$^{100\text{m}}_{39}\text{Y}$	940	30								
$^{101}_{39}\text{Y}$	426	20	325	149	149	2.3	8	3.936	1.212	1.212
$^{102}_{39}\text{Y}$	360	40	352	189	189	5.0	12	3.689	1.191	1.191
$^{102\text{m}}_{39}\text{Y}$	300	10								
$^{103}_{39}\text{Y}$	224	19	181	89	89	8.3	30	8.487	3.519	3.519
$^{104}_{39}\text{Y}$	180	60	127	30	30			11.560	3.241	3.241
$^{105}_{39}\text{Y}$			88	48	48			20.420	14.012	14.012
$^{106}_{39}\text{Y}$			66	35	35			24.010	16.345	16.345
$^{107}_{39}\text{Y}$			74	31	31			31.730	32.062	32.062
$^{108}_{39}\text{Y}$			48	23	23			25.540	36.014	36.014
$^{103}_{40}\text{Zr}$	1300	100	779	1866	1866			0.000	0.000	0.000
$^{104}_{40}\text{Zr}$	1200	300	598	1839	1839			0.012	0.023	0.023
$^{105}_{40}\text{Zr}$	600	100	289	100	100			0.127	0.029	0.029
$^{106}_{40}\text{Zr}$			270	367	367			1.476	0.614	0.614

Table 1: Continued

Isotope	$T_{1/2}$ (ms)				$P_n$ (%)					
	Exp.		KHF	QRPA-1	QRPA-2	Exp.		KHF	QRPA-1	QRPA-2
$^{107}_{40}\text{Zr}$			144	197	197			1.727	1.457	1.457
$^{108}_{40}\text{Zr}$			130	181	181			5.820	1.796	1.796
$^{109}_{40}\text{Zr}$			117	122	122			3.968	4.007	4.007
$^{110}_{40}\text{Zr}$			98	86	86			7.114	5.979	5.979
$^{103}_{41}\text{Nb}$	1500	200	3192	9535	9535			0.000	0.000	0.000
$^{104}_{41}\text{Nb}$	4900	300	1145	2790	2790	0.06	3	0.002	0.003	0.003
$^{104\text{m}}_{41}\text{Nb}$	920	40				0.05	3			
$^{105}_{41}\text{Nb}$	2950	60	1319	3864	3864	1.7	9	0.241	0.273	0.273
$^{106}_{41}\text{Nb}$	920	40	461	166	166	4.5	3	0.823	0.178	0.178
$^{107}_{41}\text{Nb}$	300	9	440	657	657	6.0	15	3.473	2.994	2.994
$^{108}_{41}\text{Nb}$	193	17	218	365	365	6.2	5	5.720	15.732	15.732
$^{109}_{41}\text{Nb}$	190	30	229	377	377	31	5	12.180	15.499	15.499
$^{110}_{41}\text{Nb}$	170	20	109	253	253	40	8	9.959	17.144	17.144
$^{111}_{41}\text{Nb}$			113	184	184			22.060	59.599	59.599
$^{112}_{41}\text{Nb}$			69	85	85			21.090	64.316	64.316
$^{113}_{41}\text{Nb}$			65	56	56			55.760	90.942	90.942
$^{109}_{42}\text{Mo}$	530	60	484	1802	1802			0.002	0.000	0.000
$^{110}_{42}\text{Mo}$	300	40	594	1832	1832			0.074	0.000	0.000
$^{111}_{42}\text{Mo}$			237	978	978			0.313	0.025	0.025
$^{112}_{42}\text{Mo}$			287	672	672			1.233	0.308	0.308
$^{113}_{42}\text{Mo}$			133	133	133			1.806	3.030	3.030
$^{114}_{42}\text{Mo}$			144	113	113			4.255	3.881	3.881
$^{115}_{42}\text{Mo}$			92	52	52			5.330	4.984	4.984
$^{108}_{43}\text{Tc}$	5170	70	1515	702	702			0.000	0.000	0.000
$^{109}_{43}\text{Tc}$	870	40	2010	378	378	0.08	2	0.017	0.008	0.008
$^{110}_{43}\text{Tc}$	920	30	663	274	274	0.04	2	0.110	0.067	0.067
$^{111}_{43}\text{Tc}$	290	20	886	195	195	0.85	20	1.367	0.327	0.327
$^{112}_{43}\text{Tc}$	290	20	312	142	142	1.5	2	1.135	0.797	0.797
$^{113}_{43}\text{Tc}$	170	20	392	115	115	2.1	3	6.418	4.536	4.536
$^{114}_{43}\text{Tc}$	150	30	172	82	82	1.3	4	4.423	7.233	7.233
$^{115}_{43}\text{Tc}$			210	74	74			13.330	19.044	19.044
$^{116}_{43}\text{Tc}$			96	46	46			11.740	16.381	16.381
$^{117}_{43}\text{Tc}$			94	42	42			22.990	24.361	24.361
$^{118}_{43}\text{Tc}$			66	36	36			17.170	25.068	25.068
$^{113}_{44}\text{Ru}$	800	50	950	2200	2200			0.000	0.000	0.000
$^{114}_{44}\text{Ru}$	530	60	1354	491	491			0.000	0.009	0.009
$^{115}_{44}\text{Ru}$	740	80	47	753	753			0.003	1.021	1.021

Table 1: Continued

Isotope	$T_{1/2}$ (ms)				$P_n$ (%)					
	Exp.	KHF	QRPA-1	QRPA-2	Exp.	KHF	QRPA-1	QRPA-2		
$^{116}_{44}\text{Ru}$		556	612	612		0.053	0.002	0.002		
$^{117}_{44}\text{Ru}$		237	175	175		0.287	0.369	0.369		
$^{118}_{44}\text{Ru}$		287	233	233		1.029	1.120	1.120		
$^{119}_{44}\text{Ru}$		162	185	185		1.712	2.616	2.616		
$^{120}_{44}\text{Ru}$		149	118	118		2.599	2.945	2.945		
$^{114}_{45}\text{Rh}$	1850	50	1244	2730	2730		0.000	0.000	0.000	
$^{114\text{m}}_{45}\text{Rh}$	1850	50								
$^{115}_{45}\text{Rh}$	990	50	476	682	682		0.083	0.016	0.016	
$^{116}_{45}\text{Rh}$	680	60	589	686	686		0.057	0.000	0.000	
$^{116\text{m}}_{45}\text{Rh}$	900	400								
$^{117}_{45}\text{Rh}$	440	40	857	245	245		1.614	0.940	0.940	
$^{118}_{45}\text{Rh}$			346	125	125		1.102	0.924	0.924	
$^{119}_{45}\text{Rh}$			411	111	111		4.196	3.203	3.203	
$^{120}_{45}\text{Rh}$			177	87	87		3.586	3.547	3.547	
$^{121}_{45}\text{Rh}$			215	65	65		11.300	7.620	7.620	
$^{122}_{45}\text{Rh}$			108	56	56		9.057	8.540	8.540	
$^{120}_{46}\text{Pd}$	500	100	1267	2686	2686		0.000	0.000	0.000	
$^{121}_{46}\text{Pd}$			428	1632	1632		0.002	0.002	0.002	
$^{122}_{46}\text{Pd}$			541	1123	1123		0.039	0.044	0.044	
$^{123}_{46}\text{Pd}$			244	476	476		0.224	0.313	0.313	
$^{124}_{46}\text{Pd}$			257	328	328		0.552	0.656	0.656	
$^{119}_{47}\text{Ag}$	2100	100	3567	985	985		0.000	0.000	0.000	
$^{119\text{m}}_{47}\text{Ag}$	6000	500								
$^{120}_{47}\text{Ag}$	1230	30	865	490	490	$\leq 0.003$	0.000	0.000	0.000	
$^{120\text{m}}_{47}\text{Ag}$	370	40								
$^{121}_{47}\text{Ag}$	780	10	1337	412	412	0.076	5	0.135	0.040	0.040
$^{122}_{47}\text{Ag}$	550	50	488	190	190	0.186	10	0.120	0.175	0.175
$^{122\text{m}}_{47}\text{Ag}$	200	50								
$^{123}_{47}\text{Ag}$	296	6	652	219	219	0.55	5	1.683	0.642	0.642
$^{124}_{47}\text{Ag}$	172	5	267	117	117	$\geq 0.1$		0.741	0.989	0.989
$^{124\text{m}}_{47}\text{Ag}$										
$^{125}_{47}\text{Ag}$	166	7	288	116	116			5.088	3.389	3.389
$^{126}_{47}\text{Ag}$	107	12	145	118	118			3.341	3.435	3.435
$^{126\text{m}}_{47}\text{Ag}$										
$^{127}_{47}\text{Ag}$	79	3	164	84	84			12.210	5.785	5.785
$^{128}_{47}\text{Ag}$	58	5	107	86	86			5.079	6.417	6.417
$^{129}_{47}\text{Ag}$	46 <sup>†</sup>	<sup>+5</sup> <sub>-9</sub>	84	33	33			11.760	8.990	8.990

<sup>†</sup>This experimental data point was added after the manuscript was completed and is therefore not taken into account elsewhere in figures and tables.

Table 1: Continued

Isotope	$T_{1/2}$ (ms)					$P_n$ (%)			
	Exp.	KHF	QRPA-1	QRPA-2		Exp.	KHF	QRPA-1	QRPA-2
$^{129m}_{47}\text{Ag}$									
$^{130}_{47}\text{Ag}$		30	36	36			19.240	67.219	67.219
$^{131}_{47}\text{Ag}$		28	40	40			68.150	100.000	100.000
$^{132}_{47}\text{Ag}$		20	34	34			61.090	100.000	100.000
$^{126}_{48}\text{Cd}$	506	15	798	5146	5146		0.000	0.000	0.000
$^{127}_{48}\text{Cd}$	370	70	280	2329	2329		0.019	0.223	0.223
$^{128}_{48}\text{Cd}$	340	30	289	924	924		0.079	0.752	0.752
$^{129}_{48}\text{Cd}$	270	40	135	2284	2284		0.766	0.944	0.944
$^{130}_{48}\text{Cd}$	162	7	138	655	655	3.6 10	1.083	2.883	2.883
$^{131}_{48}\text{Cd}$	68	3	65	545	545	3.5 10	3.855	61.210	61.210
$^{132}_{48}\text{Cd}$	97	10	56	563	563	60 15	20.210	99.976	99.976
$^{133}_{48}\text{Cd}$			38	446	446		26.530	99.025	99.025
$^{134}_{48}\text{Cd}$			38	313	313		37.150	100.000	100.000
$^{135}_{48}\text{Cd}$			28	253	253		36.370	99.407	99.407
$^{136}_{48}\text{Cd}$			30	132	132		44.050	100.000	100.000
$^{125}_{49}\text{In}$	2360	40	3247	857	857		0.000	0.000	0.000
$^{125m}_{49}\text{In}$	12200	200							
$^{126}_{49}\text{In}$	1600	100	909	552	552		0.000	0.000	0.000
$^{126m}_{49}\text{In}$	1640	50							
$^{127}_{49}\text{In}$	1090	10	1192	567	567	$\leq 0.03$	0.035	0.019	0.019
$^{127m1}_{49}\text{In}$	3670	40				0.69 4			
$^{127m2}_{49}\text{In}$									
$^{128}_{49}\text{In}$	776	24	527	480	480	0.038 3	0.023	0.027	0.027
$^{128m}_{49}\text{In}$	776	24							
$^{129}_{49}\text{In}$	611	4	525	312	312	0.23 7	0.792	0.670	0.670
$^{129m1}_{49}\text{In}$	1230	30				3.6 4			
$^{129m2}_{49}\text{In}$									
$^{130}_{49}\text{In}$	278	3	246	216	216	1.01 22	0.551	0.985	0.985
$^{130m1}_{49}\text{In}$	538	5							
$^{130m2}_{49}\text{In}$	550	10				1.65 18			
$^{131}_{49}\text{In}$	280	30	216	146	146	2.2 3	3.685	3.817	3.817
$^{131m1}_{49}\text{In}$	350	50							
$^{131m2}_{49}\text{In}$	320	60							
$^{132}_{49}\text{In}$	206	4	45	95	95	5.2 12	7.627	9.237	9.237
$^{133}_{49}\text{In}$	180	15	35	139	139	87 9	56.760	100.000	100.000
$^{134}_{49}\text{In}$	138	8	32	97	97	$> 17$	56.700	100.000	100.000
$^{135}_{49}\text{In}$			41	90	90		70.890	100.000	100.000

Table 1: Continued

Isotope	$T_{1/2}$ (ms)				$P_n$ (%)					
	Exp.	KHF	QRPA-1	QRPA-2	Exp.	KHF	QRPA-1	QRPA-2		
$^{136}_{49}\text{In}$		30	69	69		56.880	100.000	100.000		
$^{137}_{49}\text{In}$		31	48	48		79.100	100.000	100.000		
$^{133}_{50}\text{Sn}$	1450	30	362	9479	9479	0.0294	24	0.002	0.040	0.040
$^{134}_{50}\text{Sn}$	1120	80	245	2196	2196	17	14	6.000	93.128	93.128
$^{135}_{50}\text{Sn}$	450	50	215	2789	2789	22	7	12.650	98.591	98.591
$^{136}_{50}\text{Sn}$			169	904	904	25	7	9.478	88.334	88.334
$^{137}_{50}\text{Sn}$			140	733	733			16.100	99.360	99.360
$^{138}_{50}\text{Sn}$			143	460	460			32.410	100.000	100.000
$^{139}_{50}\text{Sn}$			81	338	338			18.710	99.303	99.303
$^{140}_{50}\text{Sn}$			86	119	119			27.800	99.997	99.997
$^{134}_{51}\text{Sb}$	780	60	765	88293	973552			0.014	2.032	14.190
$^{134m}_{51}\text{Sb}$	10220	90				0.088	17			
$^{135}_{51}\text{Sb}$	1680	15	385	33748	36889	22.0	27	15.210	97.980	99.948
$^{136}_{51}\text{Sb}$	923	14	302	2261	27082	23.2	68	19.440	53.683	99.789
$^{137}_{51}\text{Sb}$			199	970	4727			25.710	96.361	99.998
$^{138}_{51}\text{Sb}$			168	41	1599			28.350	26.302	99.982
$^{139}_{51}\text{Sb}$			127	176	876			35.210	99.766	100.000
$^{140}_{51}\text{Sb}$			80	38	645			36.270	58.560	99.992
$^{141}_{51}\text{Sb}$			86	84	84			65.230	99.378	99.378
$^{142}_{51}\text{Sb}$			46	45	45			40.790	95.947	95.947
$^{143}_{51}\text{Sb}$			50	29	29			62.860	99.999	99.999
$^{136}_{52}\text{Te}$	17630	80	1079	49938	49938	1.26	20	0.128	10.451	10.451
$^{137}_{52}\text{Te}$	2490	50	711	119887	151542	2.86	24	0.440	54.228	69.222
$^{138}_{52}\text{Te}$	1400	400	438	25690	25690	6.3	21	0.978	3.683	3.683
$^{139}_{52}\text{Te}$			347	269	5329			3.304	2.295	52.042
$^{140}_{52}\text{Te}$			304	282	1138			3.880	2.947	7.825
$^{141}_{52}\text{Te}$			213	122	632			4.876	8.355	44.492
$^{142}_{52}\text{Te}$			200	108	108			7.381	10.457	10.457
$^{143}_{52}\text{Te}$			105	67	67			10.320	16.262	16.262
$^{144}_{52}\text{Te}$			117	63	63			14.790	22.622	22.622
$^{145}_{52}\text{Te}$			77	30	30			14.670	21.510	21.510
$^{146}_{52}\text{Te}$			75	38	38			18.540	35.513	35.513
$^{137}_{53}\text{I}$	24130	120	1995	1894022	3365424	7.02	54	1.426	72.004	98.980
$^{138}_{53}\text{I}$	6490	70	1152	2254	9020949	5.17	36	1.092	0.858	69.824
$^{139}_{53}\text{I}$	2282	10	920	2338	58145	10.8	12	7.645	15.749	99.988
$^{140}_{53}\text{I}$	860	40	518	302	17216	14.4	63	5.825	10.850	99.728
$^{141}_{53}\text{I}$	430	20	521	351	2347	30	9	14.190	42.231	100.000

Table 1: Continued

Isotope	$T_{1/2}$ (ms)				$P_n$ (%)					
	Exp.	KHF	QRPA-1	QRPA-2	Exp.	KHF	QRPA-1	QRPA-2		
$^{142}_{53}\text{I}$		308	182	1400		10.750	46.997	99.952		
$^{143}_{53}\text{I}$		296	150	150		21.460	77.120	77.120		
$^{144}_{53}\text{I}$		194	58	58		17.370	29.379	29.379		
$^{145}_{53}\text{I}$		127	57	57		38.580	46.359	46.359		
$^{146}_{53}\text{I}$		80	29	29		24.200	27.584	27.584		
$^{147}_{53}\text{I}$		75	33	33		41.940	59.854	59.854		
$^{148}_{53}\text{I}$		55	30	30		35.650	81.555	81.555		
$^{149}_{53}\text{I}$		55	39	39		53.140	97.687	97.687		
$^{141}_{54}\text{Xe}$	1730	10	1290	725	83645	0.046	4	0.006	0.004	0.168
$^{142}_{54}\text{Xe}$	1220	20	1113	841	6634	0.42	3	0.027	0.020	0.113
$^{143}_{54}\text{Xe}$	300	30	654	464	4155			0.334	0.450	0.743
$^{144}_{54}\text{Xe}$	1150	200	647	291	291			0.651	0.693	0.693
$^{145}_{54}\text{Xe}$	900	300	417	233	233			1.510	3.805	3.805
$^{146}_{54}\text{Xe}$			369	292	292			1.973	3.397	3.397
$^{147}_{54}\text{Xe}$			260	93	93			4.300	5.438	5.438
$^{148}_{54}\text{Xe}$			176	126	126			6.168	9.592	9.592
$^{149}_{54}\text{Xe}$			119	94	94			9.234	22.899	22.899
$^{150}_{54}\text{Xe}$			112	71	71			11.440	25.968	25.968
$^{151}_{54}\text{Xe}$			83	33	33			14.180	24.373	24.373
$^{153}_{54}\text{Xe}$			0	27	27			0.000	52.705	52.705
$^{141}_{55}\text{Cs}$	24940	60	3636	9279	807516	0.038	8	0.035	0.026	4.653
$^{142}_{55}\text{Cs}$	1689	11	1731	1261	882522	0.091	8	0.121	0.031	39.801
$^{143}_{55}\text{Cs}$	1791	8	1411	1750	21384	1.59	15	1.588	1.067	30.965
$^{144}_{55}\text{Cs}$	993	13	692	1243	18073	3.41	40	1.871	3.754	66.359
$^{145}_{55}\text{Cs}$	582	6	436	412	932	13.1	7	4.884	8.146	17.980
$^{146}_{55}\text{Cs}$	323	6	381	784	784	13.4	10	10.240	36.444	36.444
$^{147}_{55}\text{Cs}$	225	5	206	234	234	27.5	21	8.264	16.383	16.383
$^{148}_{55}\text{Cs}$	158	7	207	165	165	25.0	43	21.700	34.467	34.467
$^{149}_{55}\text{Cs}$	112	3	172	219	219			19.130	64.646	64.646
$^{150}_{55}\text{Cs}$	82	7	123	158	158	20	10	18.110	71.808	71.808
$^{151}_{55}\text{Cs}$			109	101	101			27.690	82.526	82.526
$^{152}_{55}\text{Cs}$			82	30	30			27.290	47.453	47.453
$^{153}_{55}\text{Cs}$			77	56	56			38.830	89.391	89.391
$^{154}_{55}\text{Cs}$			58	43	43			33.580	83.477	83.477
$^{146}_{56}\text{Ba}$	2220	70	2538	2457	2457			0.000	0.000	0.000
$^{147}_{56}\text{Ba}$	893	1	1785	3559	3559			0.000	0.000	0.000
$^{148}_{56}\text{Ba}$	602	25	1054	603	603	0.12	6	0.062	0.076	0.076

Table 1: Continued

Isotope	$T_{1/2}$ (ms)					$P_n$ (%)				
	Exp.		KHF	QRPA-1	QRPA-2	Exp.		KHF	QRPA-1	QRPA-2
$^{149}_{56}\text{Ba}$	344	7	467	300	300	0.79	39	0.092	0.123	0.123
$^{150}_{56}\text{Ba}$	300		389	438	438	1.0	5	0.700	0.806	0.806
$^{151}_{56}\text{Ba}$			259	310	310			1.757	4.174	4.174
$^{152}_{56}\text{Ba}$			228	205	205			2.763	4.534	4.534
$^{153}_{56}\text{Ba}$			158	69	69			4.732	4.634	4.634
$^{154}_{56}\text{Ba}$			157	94	94			6.361	9.117	9.117
$^{146}_{57}\text{La}$	6270	100	3572	1212	1212			0.000	0.000	0.000
$^{146m}_{57}\text{La}$	10000	100								
$^{147}_{57}\text{La}$	4015	8	5033	13458	13458	0.032	11	0.004	0.008	0.008
$^{148}_{57}\text{La}$	1050	10	1731	15129	15129	0.153	43	0.052	0.003	0.003
$^{149}_{57}\text{La}$	1050	30	2342	2255	2255	1.46	29	0.249	1.229	1.229
$^{150}_{57}\text{La}$	510	30	1130	570	570	2.69	34	0.277	0.796	0.796
$^{151}_{57}\text{La}$			778	874	874			1.856	12.933	12.933
$^{152}_{57}\text{La}$			451	612	612			3.104	28.109	28.109
$^{153}_{57}\text{La}$			342	345	345			7.539	50.360	50.360
$^{154}_{57}\text{La}$			228	96	96			9.276	20.237	20.237
$^{155}_{57}\text{La}$			184	142	142			17.560	59.075	59.075
$^{156}_{57}\text{La}$			112	103	103			18.900	60.043	60.043
$^{152}_{58}\text{Ce}$	1100	300	1831	3169	3169			0.000	0.000	0.000
$^{153}_{58}\text{Ce}$			979	1814	1814			0.000	0.018	0.018
$^{154}_{58}\text{Ce}$			775	870	870			0.019	0.095	0.095
$^{155}_{58}\text{Ce}$			471	174	174			0.257	0.180	0.180
$^{156}_{58}\text{Ce}$			369	306	306			0.697	0.734	0.734
$^{152}_{59}\text{Pr}$	3630	120	3746	965	965			0.000	0.000	0.000
$^{153}_{59}\text{Pr}$	4300	200	2607	863	863			0.000	0.001	0.001
$^{154}_{59}\text{Pr}$	2300	100	1539	542	542			0.048	0.169	0.169
$^{155}_{59}\text{Pr}$			852	359	359			0.367	0.150	0.150
$^{156}_{59}\text{Pr}$			733	144	144			2.325	1.336	1.336
$^{157}_{59}\text{Pr}$			598	165	165			3.776	7.694	7.694
$^{156}_{60}\text{Nd}$	5470	110	3229	7086	7086			0.000	0.000	0.000
$^{157}_{60}\text{Nd}$			1906	508	508			0.000	0.000	0.000
$^{158}_{60}\text{Nd}$			1331	1313	1313			0.000	0.000	0.000
$^{159}_{60}\text{Nd}$			773	772	772			0.021	0.026	0.026
$^{157}_{61}\text{Pm}$	10560	100	8084	2101	2101			0.000	0.000	0.000
$^{158}_{61}\text{Pm}$	4800	500	4496	488	488			0.000	0.000	0.000
$^{159}_{61}\text{Pm}$			2623	642	642			0.002	0.006	0.006
$^{160}_{61}\text{Pm}$			1561	493	493			0.073	0.049	0.049

Table 1: Continued

Isotope	$T_{1/2}$ (ms)					$P_n$ (%)			
	Exp.		KHF	QRPA-1	QRPA-2	Exp.	KHF	QRPA-1	QRPA-2
$^{161}_{61}\text{Pm}$			1065	331	331		0.803	0.361	0.361
$^{160}_{62}\text{Sm}$	9600	300	9440	26147	26147		0.000	0.000	0.000
$^{161}_{62}\text{Sm}$	4800		4442	11207	11207		0.000	0.000	0.000
$^{162}_{62}\text{Sm}$			3099	6821	6821		0.000	0.000	0.000
$^{163}_{62}\text{Sm}$			1748	3580	3580		0.000	0.000	0.000
$^{164}_{62}\text{Sm}$			1226	2527	2527		0.001	0.000	0.000
$^{165}_{62}\text{Sm}$			764	701	701		0.066	0.020	0.020
$^{166}_{62}\text{Sm}$			570	624	624		0.288	0.469	0.469
$^{162}_{63}\text{Eu}$	10600	1000	9218	40430	40430		0.000	0.000	0.000
$^{163}_{63}\text{Eu}$			5219	23562	23562		0.000	0.000	0.000
$^{164}_{63}\text{Eu}$			2844	12047	12047		0.001	0.000	0.000
$^{165}_{63}\text{Eu}$			1794	7521	7521		0.117	0.144	0.144

used Mainz  $4\pi$  neutron detector consists of  $64\ ^3\text{He}$  proportional counters arranged in three concentric rings in a large, well-shielded paraffin matrix (Böhmer, 1998) with a total efficiency of about 45 %. The majority of the new  $P_n$  values were deduced from the ratios of simultaneously measured  $\beta$ - and delayed-neutron activities. It was only in a few cases that  $\gamma$ -spectroscopic data were used to determine the one or other decay property (e.g. independent  $P_n$  determinations for  $^{93}\text{Br}$ ,  $^{100}\text{Rb}$  and  $^{135}\text{Sn}$ ). Most of the new data were obtained at the on-line mass-separator facility ISOLDE at CERN (see, e.g. Fedoseyev *et al.*, 1995; Kratz *et al.*, 2000; Hannawald *et al.*, 2000; Köster, 2000; Shergur *et al.*, 2000). Data in the Fe-group region were obtained at the fragment separators LISE at GANIL (Dörfler *et al.*, 1996; Sorlin *et al.*, 2000) and FRS at GSI (Ameil *et al.*, 1998; Bernas *et al.*, 1998), and at the LISOL separator at Louvain-la-Neuve (Franchoo *et al.*, 1998; Weissman *et al.*, 1999; Mueller *et al.*, 2000). Data in the refractory-element region were measured at the ion-guide separator IGISOL at Jyväskylä (Mehren *et al.*, 1996; Wang *et al.*, 1999). Finally, some new data in the  $^{132}\text{Sn}$  region came from the OSIRIS mass-separator group at Studsvik (Korgul *et al.*, 2000; Mach *et al.*, 2000).

In a number of cases, “old”  $P_n$  values from the 1970’s deduced from measured delayed-neutron yields and (questionable) fission yields not yet containing the later well established odd-even effects, were – as far as possible – corrected, as was also done by Rudstam in his 1993 compilation (Rudstam, 1993). In those cases, where later publications explicitly stated that the new data supersede earlier ones, the latter were no longer taken into account. Multiple determinations of the same isotopes performed with the same method at the same facility by the same authors (e.g. for Rb and Cs precursors) were treated differently from the common practice to calculate weighted averages of experimental values, when a later measurement was more reliable than earlier ones. Finally, a number of “questionable”  $P_n$  values, in particular those where no modern mass model would predict the ( $Q_\beta - S_n$ ) window for neutron emission to be positive (e.g.  $^{146,147}\text{Ba}$  and  $^{146}\text{La}$ ), are still cited in our Table,

but should in fact be neglected in any application, hence also in reactor calculations.

## MODELS

Theoretically, both integral  $\beta$ -decay quantities,  $T_{1/2}$  and  $P_n$ , are interrelated via their usual definition in terms of the so-called  $\beta$ -strength function ( $S_\beta(E)$ ) (see, e.g. Duke *et al.* (1970)).

$$1/T_{1/2} = \sum_{E_i \geq 0}^{E_i \leq Q_\beta} S_\beta(E_i) \times f(Z, Q_\beta - E_i); \quad (1)$$

where  $Q_\beta$  is the maximum  $\beta$ -decay energy (or the isobaric mass difference) and  $f(Z, Q_\beta - E_i)$  the Fermi function. With this definition,  $T_{1/2}$  may yield information on the *average*  $\beta$ -feeding of a nucleus. However, since the low-energy part of its excitation spectrum is strongly weighted by the energy factor of  $\beta$ -decay,  $f \sim (Q_\beta - E_i)^5$ ,  $T_{1/2}$  is dominated by the lowest-energy resonances in  $S_\beta(E_i)$ ; i.e. by the (near-) ground-state allowed (Gamow-Teller, GT) or first-forbidden (ff) transitions.

The  $\beta$ -delayed neutron emission probability ( $P_n$ ) is schematically given by

$$P_n = \frac{\sum_{B_n}^{Q_\beta} S_\beta(E_i) f(Z, Q_\beta - E_i)}{\sum_0^{Q_\beta} S_\beta(E_i) f(Z, Q_\beta - E_i)} \quad (2)$$

thus defining  $P_n$  as the ratio of the integral  $\beta$ -strength to states above the neutron separation energy  $S_n$ . As done in nearly all  $P_n$  calculations, in the above equation, the ratio of the partial widths for l-wave neutron emission ( $\Gamma_n^j(E_n)$ ) and the total width ( $\Gamma_{\text{tot}} = \Gamma_n^j(E_n) + \Gamma_\gamma$ ) is set equal to 1; i.e. possible  $\gamma$ -decay from neutron-unbound levels is neglected. As we will discuss later, this simplification is justified in most but not all delayed-neutron decay (precursor – emitter – final nucleus) systems. In any case, again because of the  $(Q_\beta - E)^5$  dependence of the Fermi function, the physical significance of the  $P_n$  quantity is limited, too. It mainly reflects the  $\beta$ -feeding to the energy region just beyond  $S_n$ . Taken together, however, the two gross decay properties,  $T_{1/2}$  **and**  $P_n$ , may well provide some first information about the nuclear structure determining  $\beta$ -decay. Generally speaking, for a given  $Q_\beta$  value a *short* half-life usually correlates with a *small*  $P_n$  value, and vice versa. This is actually more than a rule of thumb since it can be used to check the consistency of experimental numbers. Sometimes even global plots of double-ratios of experimental to theoretical  $P_n$  to  $T_{1/2}$  relations are used to show systematic trends (see, e.g. Tachibana *et al.* (1998)). Concerning the identification of special nuclear-structure features only from  $T_{1/2}$  and  $P_n$ , there are several impressive examples in literature. Among them are: (i) the development of single-particle (SP) structures and related ground-state shape changes in the  $50 \leq N \leq 60$  region of the Sr isotopes (Kratz, 1984), (ii) the at that time totally unexpected prediction of collectivity of neutron-magic ( $N=28$ )  $^{44}\text{S}$  situated two proton-pairs below the doubly-magic  $^{48}\text{Ca}$  (Sorlin *et al.*, 1993), and (iii) the very recent interpretation of the surprising decay properties of  $^{131,132}\text{Cd}$  just above  $N = 82$  (Kratz *et al.*, 2000; Hannawald *et al.*, 2000).

Today, in studies of nuclear-structure features, even of gross properties such as the  $T_{1/2}$  and  $P_n$  values considered here, a substantial number of different theoretical approaches are used. The significance and sophistication of these models and their relation to each other

should, however, be clear before they are applied. Therefore, in the following we assign the nuclear models used to calculate the above two decay properties to different groups:

1. *Models where the physical quantity of interest is given by an expression such as a polynomial or an algebraic expression.*

Normally, the parameters are determined by adjustments to experimental data and describe only a single nuclear property. No nuclear wave functions are obtained in these models. Examples of theories of this type are purely empirical approaches that assume a specific shape of  $S_\beta(E)$  (either constant or proportional to level density), such as the Kratz-Herrmann formula (Kratz and Herrmann, 1973) or the statistical "gross theory" of  $\beta$ -decay (Takahashi, 1972; Takahashi *et al.*, 1973). These models can be considered to be analogous to the liquid-drop model of nuclear masses, and are—again—appropriate for dealing with *average* properties of  $\beta$ -decay, however taking into account the Ikeda sum-rule to quantitatively define the total strength. In both types of approaches, model-inherently no insight into the underlying single-particle (SP) structure is possible.

2. *Models that use an effective nuclear interaction and usually solve the microscopic quantum-mechanical Schrödinger or Dirac equation.*

The approaches that actually solve the Schrödinger equation provide nuclear wave functions which allow a variety of nuclear properties (e.g. ground-state shapes, level energies, spins and parities, transition rates,  $T_{1/2}$ ,  $P_{xn}$ , etc.) to be modeled within a single framework. Most theories of this type that are currently used in large-scale calculations, such as e.g. the FRDM+QRPA model used here (Möller *et al.*, 1997) or the ETFSI+cQRPA approach (Aboussir *et al.*, 1995; Borzov *et al.*, 1996), in principle fall into two subgroups, depending on the type of microscopic interaction used. Another aspect of these models is, whether they are restricted to spherical shapes, or to even-even isotopes, or whether they can describe **all** nuclear shapes and **all** types of nuclei:

- (a) SP approaches that use a simple central potential with additional residual interactions. The Schrödinger equation is solved in a SP approximation and additional two-body interactions are treated in the BCS, Lipkin-Nogami, or RPA approximations, for example. To obtain the nuclear potential energy as a function of shape, one combines the SP model with a macroscopic model, which then leads to the macroscopic-microscopic model. Within this approach, the nuclear ground-state energy is calculated as a sum of a microscopic correction obtained from the SP levels by use of the Strutinsky method and a macroscopic energy.
- (b) Hartree-Fock-type models, in which the postulated effective interaction is of a two-body type. If the microscopic Schrödinger equation is solved then the wave functions obtained are antisymmetrized Slater determinants. In such models, it is possible to obtain the nuclear ground-state energy as  $E = \langle \Psi_0 | H | \Psi_0 \rangle$ , otherwise the HF have many similarities to those in category 2a but have fewer parameters.

In principle, models in group 2b are expected to be more accurate, because the wave functions and effective interactions can in principle be more realistic. However, two problems

still remain today: what effective interaction is sufficiently realistic to yield more accurate results, and what are the optimized parameter values for such a two-body interaction?

Some models in category 2 have been overparameterized, which means that their microscopic origins have been lost and the results are just parameterizations of the experimental data. Examples of such models are the calculations of Hirsch *et al.* (1992, 1996) where the strength of the residual GT interaction has been fitted for each element (Z-number) in order to obtain optimum reproduction of known  $T_{1/2}$  and  $P_n$  values in each isotopic chain.

To conclude this section, let us emphasize that there is no “correct” model in nuclear physics. Any modeling of nuclear-structure properties involves approximations of the true forces and equations with the goal to obtain a formulation that can be solved in practice, but that “retains the essential features” of the true system under study, so that one can still learn something. What we mean by this, depends on the actual circumstances. It may well turn out that when proceeding from a simplistic, macroscopic approach to a more microscopic model, the first overall result may be “worse” just in terms of agreement between calculated and measured data. However, the disagreements may now be understood more easily, and further nuclear-structure-based, realistic improvements will become possible.

#### PREDICTION OF $P_n$ AND $T_{1/2}$ VALUES FROM KHF

As outlined above, Kratz and Herrmann in 1972 (Kratz and Herrmann, 1973) applied the concept of the  $\beta$ -strength function to the integral quantity of the delayed-neutron emission probability, and derived a simple phenomenological expression for  $P_n$  values, later commonly referred to as the “Kratz-Herrmann Formula”

$$P_n \simeq a[(Q_\beta - S_n)/(Q_\beta - C)]^b \quad [\%] \quad (3)$$

where  $a$  and  $b$  are free parameters to be determined by a log-log fit, and  $C$  is the cut-off parameter (corresponding to the pairing-gap according to the even and odd character of the  $\beta$ -decay daughter, i.e. the neutron-emitter nucleus).

This KHF has been used in evaluations and in generation of data files (e.g. the ENDF/B versions) for nuclear applications up to present. The above free parameters  $a$  and  $b$  were from time to time redetermined (Mann *et al.*, 1984; Mann, 1986; England *et al.*, 1986) as more experimental data became available. These values are summarized in Table 2. Using the present data set presented in Table 1, we now again obtain new  $a$  and  $b$  parameters from (i) a linear regression, and (ii) a weighted non-linear least-squares fit to about 110 measured  $P_n$  values in the fission-product region. For the present fits, the mass excesses to calculate  $Q_\beta$  and  $S_n$  were taken from the compilation of Audi and Wapstra (1995), otherwise from the FRDM model predictions (Möller *et al.*, 1995). The cut-off parameter  $C$  was calculated according to the expressions given by of Madland and Nix (1988). With the considerably larger database available today, apart from global fits of the whole  $27 \leq Z \leq 57$  fission-product region, also separate fits of the light and heavy mass regions may for the first time be of some significance. The corresponding fits to the experimental  $P_n$  values in the different mass regions are shown in Figs. 1–3, and the resulting values of the quantities  $a$  and  $b$  are given in Table 3. It is quite evident from both the Figures and the Tables, that the new fit parameters differ significantly from the earlier ones; however, no clear trend

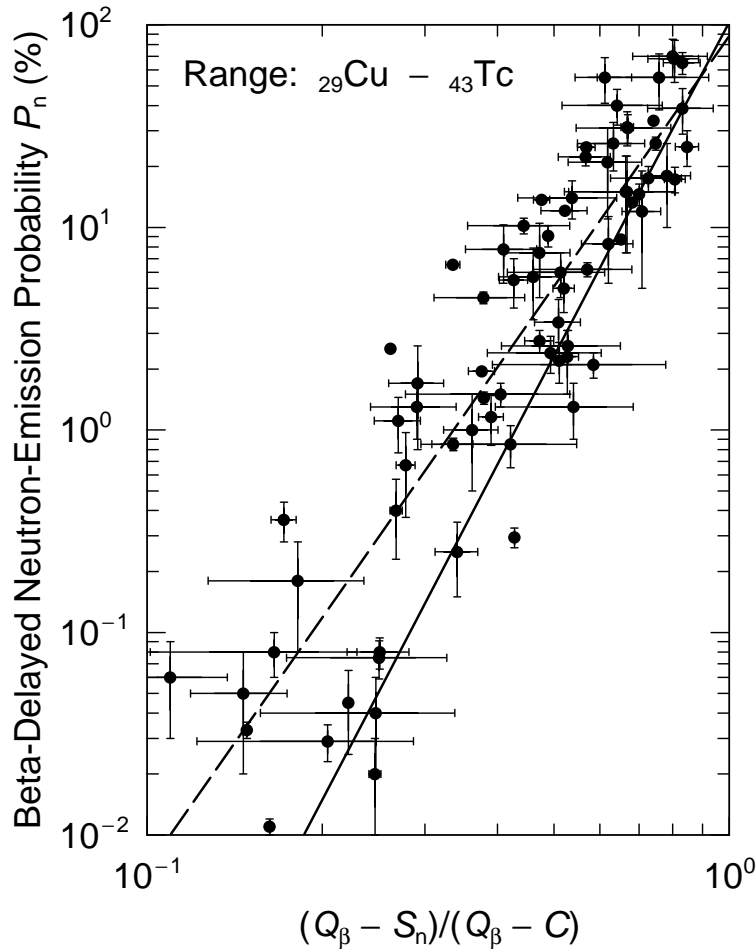


Figure 2: Fits to the Kratz-Herrmann-Formula in the region of “light” fission products. The measured  $P_n$  values (dots) are displayed as functions of the reduced energy window for delayed neutron emission. The dotted line is derived from a linear regression, whereas the full line is obtained by a weighted non-linear least-squares procedure. For the fit parameters, see Table 3.

with the increasing number of experimental data over the years is visible. With respect to the present fits, one can state that – within the given uncertainties – parameter  $a$  does not change very much, neither as a function of mass region, nor between the linear regression and the non-linear least-squares fit. However, for the slope-parameter  $b$  there is a difference. Here, the least-squares fit consistently results in a somewhat steeper slope (by about one unit) than does the linear regression.

Based on the new non-linear least-squares fit parameters, the KHF was used to predict so far unknown  $P_n$  values between  $^{27}\text{Co}$  and  $^{63}\text{Eu}$  in the relevant mass ranges for each isotopic chain. These theoretical values are listed in Table 1.

In analogy with the  $P_n$  values, the  $\beta$ -decay half-lives  $T_{1/2}$  are to be regarded as “gross”

Table 2: Parameters from fits to the Kratz–Herrmann–Formula from literature. The two sets from Kratz and Herrmann (1973) derive from different atomic mass evaluations.

Reference	Parameters	
	$a$ [%]	$b$
Kratz and Herrmann (1973)	25.	$2.1 \pm 0.2$
Kratz and Herrmann (1973)	51.	$3.6 \pm 0.3$
Mann (1984)	123.4	4.34
Mann (1986)	$54.0 +31/-20$	$3.44 \pm 0.51$
England (1986)	44.08	4.119

properties. Therefore, one can assume that the statistical concepts underlying the Kratz–Herrmann-formula for  $P_n$  values can be applied for the description of  $T_{1/2}$ .

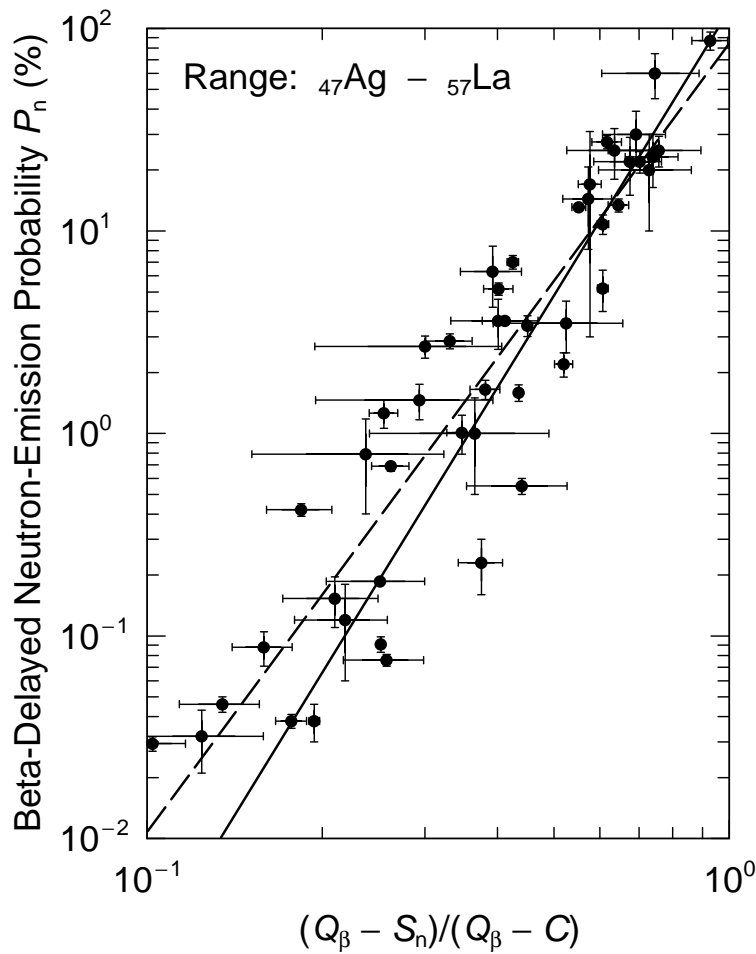


Figure 3: Fits to the Kratz-Herrmann-Formula in the region of “heavy” fission products. For an explanation of symbols, see Fig. 2.

Table 3: Parameters from fits to the Kratz–Herrmann–Formula in different mass regions. The sequence corresponds to Figs. 1 to 3.

Region	Lin. regression			Least-squares fit		
	$a$ [%]	$b$	$r^2$	$a$ [%]	$b$	red. $\chi^2$
$29 \leq Z \leq 43$	88.23	4.11	0.81	105.76 $\pm 37.67$	5.51 $\pm 0.61$	80.97
$47 \leq Z \leq 57$	84.35	3.89	0.86	123.09 $\pm 41.17$	4.68 $\pm 0.38$	57.49
$29 \leq Z \leq 57$	85.16	3.99	0.83	80.58 $\pm 20.72$	4.72 $\pm 0.34$	78.23

The half-lives are inversely proportional to the Fermi-function  $f(Z, E)$ , which, in first order, is proportional to the fifth power of the reaction  $Q_\beta$ -value:

$$T_{1/2} \sim 1/f(Z, E) \sim Q_\beta^{-5} \tag{4}$$

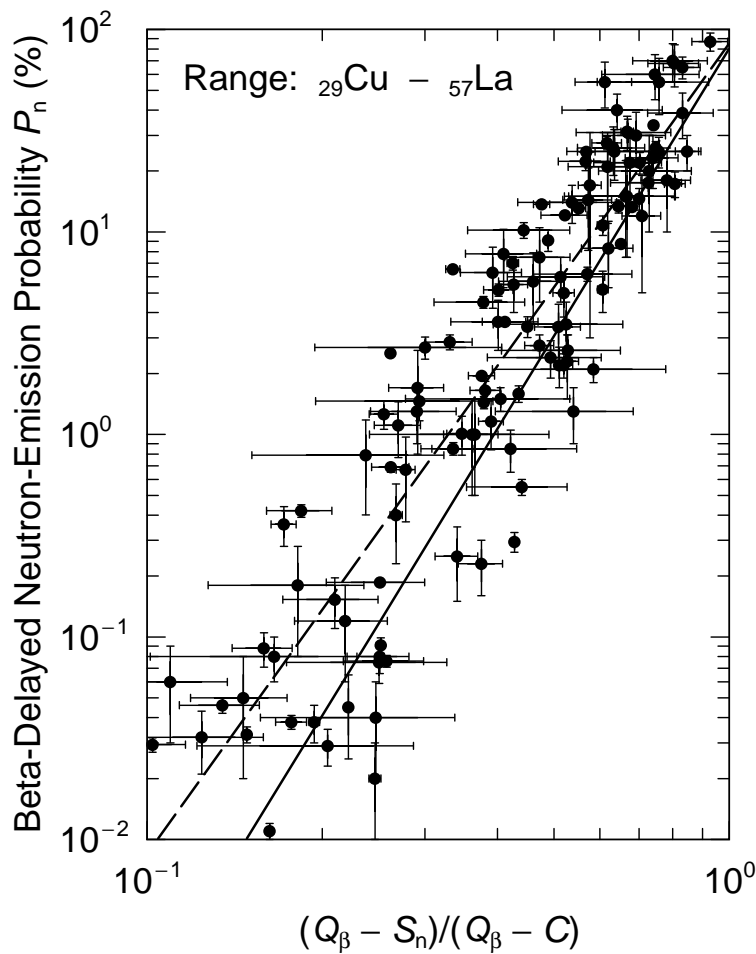


Figure 4: Fits to the Kratz-Herrmann-Formula for all fission products. For an explanation of symbols, see Fig. 2.

Table 4: Parameters from fits to  $T_{1/2}$  of neutron-rich nuclides.

lin. regression			least-squares fit		
$a$ [ms]	$b$	$r^2$	$a$ [ms]	$b$	red. $\chi^2$
2.74E06	4.5	0.72	7.07E05	4.0	1.1E04
			$\pm 5.33E05$	$\pm 0.4$	

Therefore, in a log-log plot of  $T_{1/2}$  versus  $Q_\beta$  one expects the data points to be scattered around a line with a slope of about  $-(1/5)$ .

Pfeiffer *et al.* (2000) suggested to fit the  $T_{1/2}$  of neutron-rich nuclides according to the following expression:

$$T_{1/2} \simeq a \times (Q_\beta - C)^{-b} \quad (5)$$

where the cut-off parameter  $C$  is calculated according to the fit of Madland and Nix (1988), and the parameters  $a$  and  $b$  are listed in Table 4.

The gross theory has, basically, the same functional dependence on the  $Q_\beta$ -value, but underestimates the  $\beta$ -strength to low-lying states, which results in too long half-lives. We here compensate for this deficiency by treating the coefficient  $a$  as a free parameter to be determined by a fitting procedure. The values obtained are listed in Table 1.

#### PREDICTION OF $T_{1/2}$ AND $P_n$ VALUES FROM FRDM-QRPA

The formalism we use to calculate Gamow-Teller (GT)  $\beta$ -strength functions is fairly lengthy, since it involves adding pairing and Gamow-Teller residual interactions to the folded-Yukawa single-particle Hamiltonian and solving the resulting Schrödinger equation in the quasi-particle random-phase approximation (QRPA). Because this model has been completely described in two previous papers (Krumlinde *et al.*, 1984; Möller *et al.*, 1990), we refer to those two publications for a full model specification and for a definition of notation used. We restrict the discussion here to an overview of features that are particularly relevant to the results discussed in this paper.

It is well known that wave functions and transition matrix elements are more affected by small perturbations to the Hamiltonian than are the eigenvalues. When transition rates are calculated it is therefore necessary to add residual interactions to the folded-Yukawa single-particle Hamiltonian in addition to the pairing interaction that is included in the mass model. Fortunately, the residual interaction may be restricted to a term specific to the particular type of decay considered. To obtain reasonably accurate half-lives it is also very important to include ground-state deformations. Originally the QRPA formalism was developed for and applied only to spherical nuclei (Hamamoto, 1965; Halbleib *et al.*, 1967). The extension to deformed nuclei, which is necessary in global calculations of  $\beta$ -decay properties, was first described in 1984 (Krumlinde *et al.*, 1984).

To treat Gamow-Teller  $\beta$  decay we therefore add the Gamow-Teller force

$$V_{\text{GT}} = 2\chi_{\text{GT}} : \boldsymbol{\beta}^{1-} \cdot \boldsymbol{\beta}^{1+} : \quad (6)$$

to the folded-Yukawa single-particle Hamiltonian, after pairing has already been incorporated, with the standard choice  $\chi_{\text{GT}} = 23 \text{ MeV}/A$  (Hamamoto, 1965; Halbleib *et al.*, 1967; Krumlinde *et al.*, 1984; Möller *et al.*, 1990). Here  $\beta^{1\pm} = \sum_i \sigma_i t_i^{\pm}$  are the Gamow-Teller  $\beta^{\pm}$ -transition operators.

The process of  $\beta$  decay occurs from an initial ground state or excited state in a mother nucleus to a final state in the daughter nucleus. For  $\beta^-$  decay, the final configuration is a nucleus in some excited state or its ground state, an electron (with energy  $E_e$ ), and an anti-neutrino (with energy  $E_\nu$ ). The decay rate  $w_{fi}$  to one nuclear state  $f$  is

$$w_{fi} = \frac{m_0 c^2}{\hbar} \frac{\Gamma^2}{2\pi^3} |M_{fi}|^2 f(Z, R, \epsilon_0) \quad (7)$$

where  $R$  is the nuclear radius and  $\epsilon_0 = E_0/m_0 c^2$ , with  $m_0$  the electron mass. Moreover,  $|M_{fi}|^2$  is the nuclear matrix element, which is also the  $\beta$ -strength function. The dimensionless constant  $\Gamma$  is defined by

$$\Gamma \equiv \frac{g}{m_0 c^2} \left( \frac{m_0 c}{\hbar} \right)^3 \quad (8)$$

where  $g$  is the Gamow-Teller coupling constant. The quantity  $f(Z, R, \epsilon_0)$  has been extensively discussed and tabulated elsewhere (Preston, 1962; Gove and Martin, 1971; deShalit and Feshbach, 1974).

For the special case in which the two-neutron separation energy  $S_{2n}$  in the daughter nucleus is greater than  $Q_\beta$ , the energy released in ground-state to ground-state  $\beta$  decay, the probability for  $\beta$ -delayed one-neutron emission, in percent, is given by

$$P_{1n} = 100 \frac{\sum_{S_{1n} < E_f < Q_\beta} w_{fi}}{\sum_{0 < E_f < Q_\beta} w_{fi}} \quad (9)$$

where  $E_f = Q_\beta - E_0$  is the excitation energy in the daughter nucleus and  $S_{1n}$  is the one-neutron separation energy in the daughter nucleus. We assume that decays to energies above  $S_{1n}$  always lead to delayed neutron emission.

To obtain the half-life with respect to  $\beta$  decay one sums up the decay rates  $w_{fi}$  to the individual nuclear states in the allowed energy window. The half-life is then related to the total decay rate by

$$T_\beta = \frac{\ln 2}{\sum_{0 < E_f < Q_\beta} w_{fi}} \quad (10)$$

The above equation may be rewritten as

$$T_\beta = \frac{\hbar}{m_0 c^2} \frac{2\pi^3 \ln 2}{\Gamma^2} \frac{1}{\sum_{0 < E_f < Q_\beta} |M_{fi}|^2 f(Z, R, \epsilon_0)} = \frac{B}{\sum_{0 < E_f < Q_\beta} |M_{fi}|^2 f(Z, R, \epsilon_0)} \quad (11)$$

with

$$B = \frac{\hbar}{m_0 c^2} \frac{2\pi^3 \ln 2}{\Gamma^2} \quad (12)$$

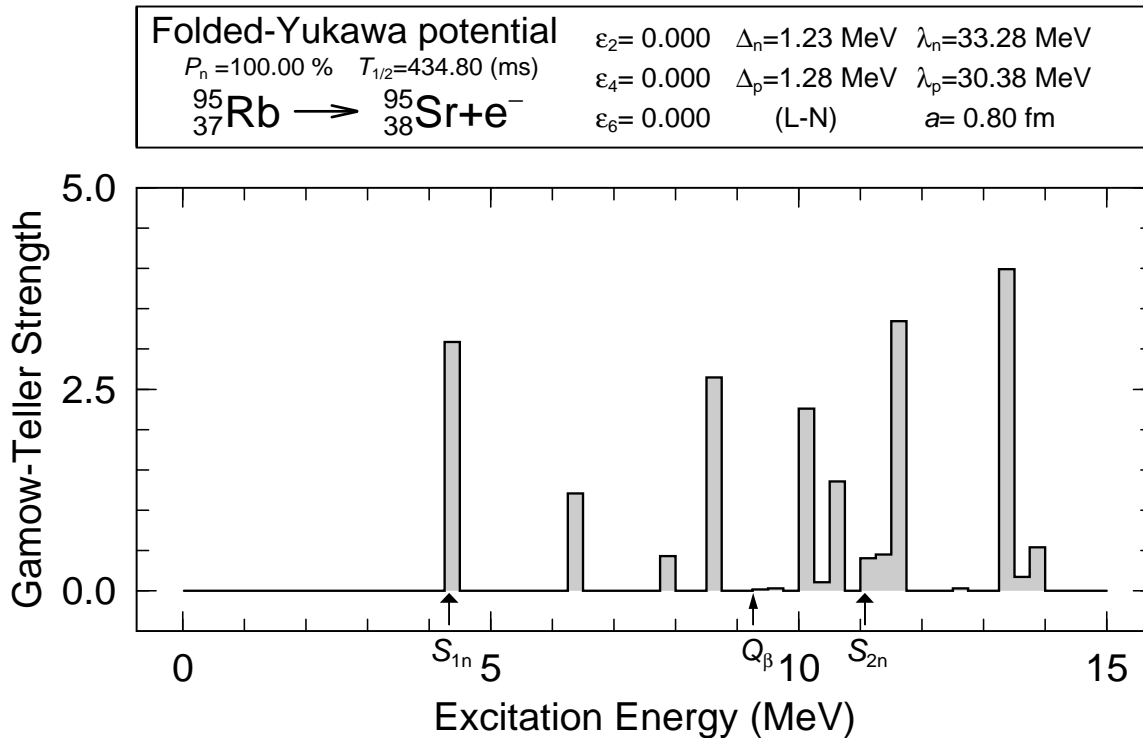


Figure 5: Calculated  $\beta$ -strength function for  ${}^{95}\text{Rb}$  in our standard model (Möller *et al.*, 1997). However, the deformation is not taken from the standard ground-state mass and deformation calculation (Möller *et al.*, 1995). Instead the ground-state shape is assumed spherical, in accordance with experimental evidence. The figure shows the sensitivity of the calculated  $P_n$  value to small details of the model. Since there is no strength below the neutron separation energy, the calculated  $\beta$ -delayed neutron-emission probability is 100%. However it is clear from the figure that just a small decrease in the energy of the large peak just above the neutron binding energy would drastically change the calculated value.

For the value of  $B$  corresponding to Gamow-Teller decay we use

$$B = 4131 \text{ s} \quad (13)$$

The energy released in ground-state to ground-state electron decay is given in terms of the atomic mass excess  $M(Z, N)$  or the total binding energy  $E_{\text{bind}}(Z, N)$  by

$$Q_{\beta\Gamma} = M(Z, N) - M(Z + 1, N - 1) \quad (14)$$

The above formulas apply to the  $\beta^-$  decays that are of interest here. The decay  $Q$  values and neutron separation energies  $S_{\nu n}$  are obtained from our FRDM mass model when experimental data are unavailable (Möller *et al.*, 1995). The matrix elements  $M_{fi}$  are obtained from our QRPA model. More details are provided elsewhere (Möller *et al.*, 1990).

We present here two calculations, QRPA-1 and QRPA-2 of  $T_{1/2}$  and  $P_n$ . They are based on our standard QRPA model described above, but with the following enhancements:

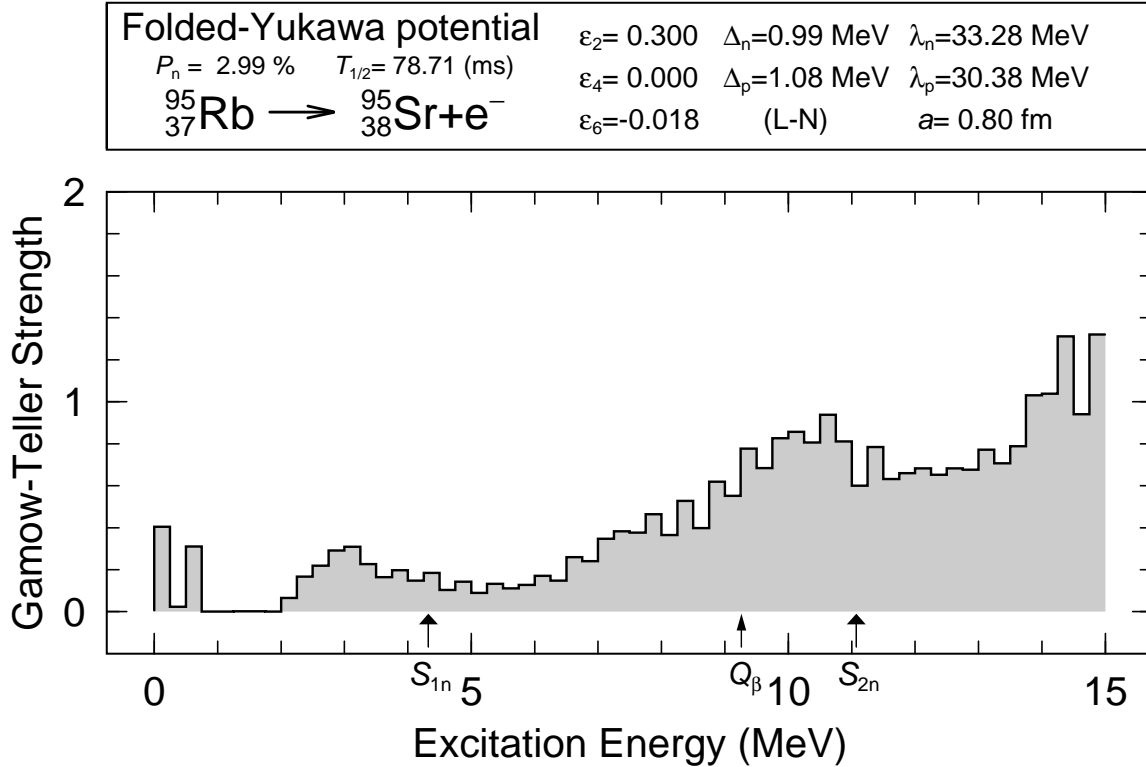


Figure 6: This calculation corresponds to the **QRPA-1** model specification. However, this nucleus is known to be spherical although a deformed shape was obtained in the ground-state mass-and-deformation calculation (Möller *et al.*, 1995). Therefore, in our **QRPA-2** calculation in Fig. 7, this nucleus is treated as spherical in accordance with experiment.

#### For QRPA-1:

1. To calculate  $\beta$ -decay  $Q$ -values and neutron separation energies  $S_{\nu n}$  we use experimental ground-state masses where available, otherwise calculated masses (Möller *et al.*, 1995). In our previous recent calculations we used the 1989 mass evaluation (Audi 1989); here we use the 1995 mass evaluation (Audi *et al.*, 1995).
2. It is known that at higher excitation energies additional residual interactions result in a spreading of the transition strength. In our 1997 calculation each transition goes to a precise, well-specified energy in the daughter nucleus. This can result in very large changes in the calculated  $P_n$  values for minute changes in, for example  $S_{1n}$ , depending on whether an intense, sharp transition is located just below or just above the neutron separation energy (Möller *et al.*, 1990). To remove this unphysical feature we introduce an empirical spreading width that sets in above 2 MeV. Specifically, each transition strength “spike” above 2 MeV is transformed to a Gaussian of width

$$\Delta_{\text{sw}} = \frac{8.62}{A^{0.57}} \quad (15)$$

This choice is equal to the error in the mass model. Thus, it accounts approximately for the uncertainty in calculated neutron separation energies

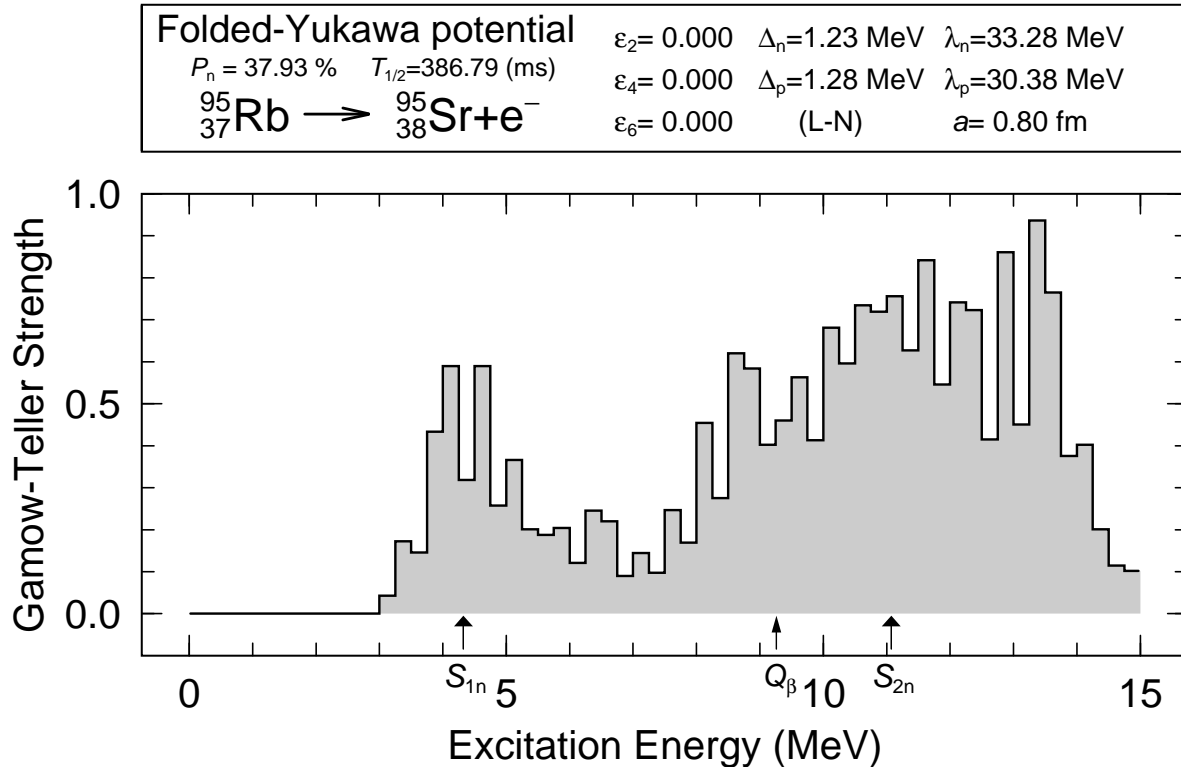


Figure 7: This calculation corresponds to the **QRPA-2** model specification. The calculation is identical to the calculation in Fig. 6 except that the ground-state shape here is spherical.

and at the same time it roughly corresponds to the observed spreading of transition strengths in the energy range 2–10 MeV, which is the range of interest here.

#### For QRPA-2:

1. In this calculation we retain all of the features of the QRPA-1 calculation and in addition account more accurately for the ground-state deformations which affect the energy levels and wave-functions that are obtained in the single-particle model. The ground-state deformations calculated in the FRDM mass model (Möller *et al.*, 1992), generally agree with experimental observations, but in transition regions between spherical and deformed nuclei discrepancies do occur. In the QRPA-2 calculation we therefore replace calculated deformations with spherical shape, when experimental data so indicate. This has been done for the following nuclei:  
 ${}^{67-78}\text{Fe}$ ,  ${}^{67-79}\text{Co}$ ,  ${}^{73-80}\text{Ni}$ ,  ${}^{73-81}\text{Cu}$ ,  ${}^{78-84}\text{Zn}$ ,  ${}^{79-87}\text{Ga}$ ,  ${}^{83-90}\text{Ge}$ ,  ${}^{84-91}\text{As}$ ,  ${}^{87-94}\text{Se}$ ,  
 ${}^{87-96}\text{Br}$ ,  ${}^{92-98}\text{Kr}$ ,  ${}^{91-96}\text{Rb}$ ,  ${}^{96-97}\text{Sr}$ ,  ${}^{96-98}\text{Y}$ ,  ${}^{134-140}\text{Sb}$ ,  ${}^{136-141}\text{Te}$ ,  ${}^{137-142}\text{I}$ ,  
 ${}^{141-143}\text{Xe}$ , and  ${}^{141-145}\text{Cs}$ .

To illustrate some typical features of  $\beta$ -strength functions we present the strength function of  ${}^{95}\text{Rb}$  calculated in three different ways in Figs. 5–7.

It is not our aim here to make a detailed analysis of each individual nucleus, but instead to present an overview of the model performance in a calculation of

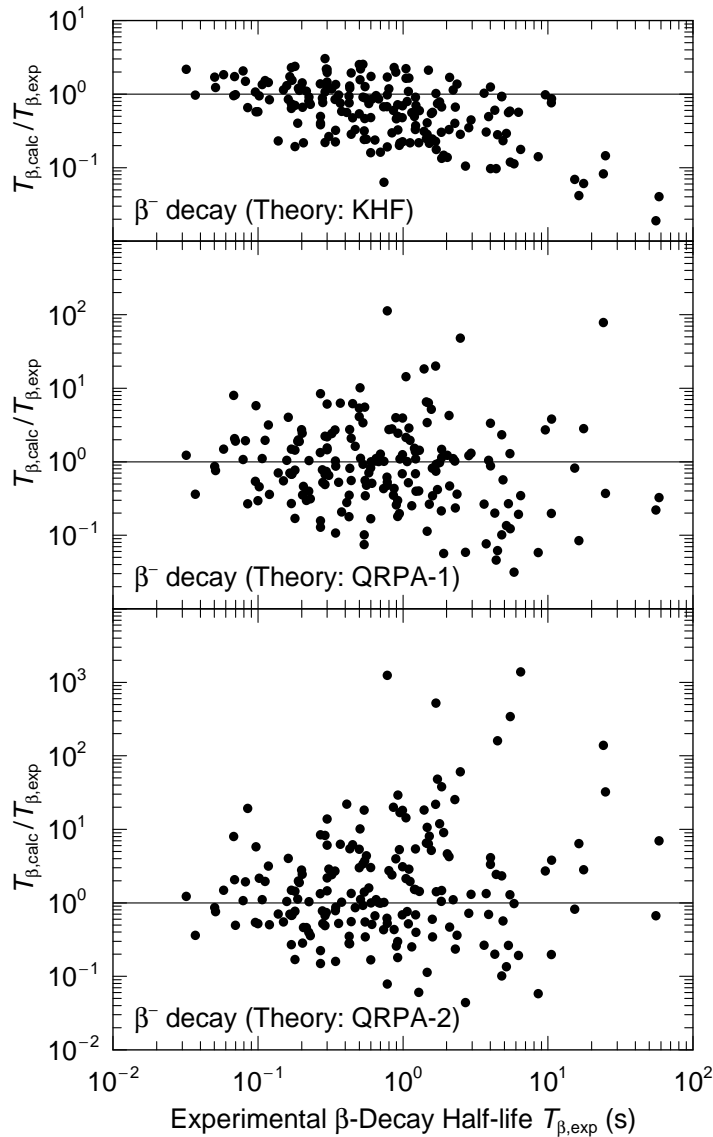


Figure 8: Ratio of calculated to experimental  $\beta$ -decay half-lives for nuclei in the fission-product region in three different models.

a large number of  $\beta$ -decay half-lives. In Figs. 8 and 9 we compare measured and calculated  $\beta$ -decay half-lives and  $\beta$ -delayed neutron emission probabilities for the nuclei considered here. To address the reliability in various regions of nuclei and versus distance from stability, we present the ratios  $T_{\beta,\text{calc}}/T_{\beta,\text{exp}}$   $P_{n,\text{calc}}/P_{n,\text{exp}}$  versus the quantity  $T_{\beta,\text{exp}}$ . Because the relative error in the calculated half-lives is more sensitive to small shifts in the positions of the calculated single-particle levels for decays with small energy releases, where long half-lives are expected, one can anticipate that half-life calculations are more reliable far from stability than close to  $\beta$ -stable nuclei.

Before we make a quantitative analysis of the agreement between calculated and experimental half-lives we briefly discuss what conclusions can be drawn from a simple

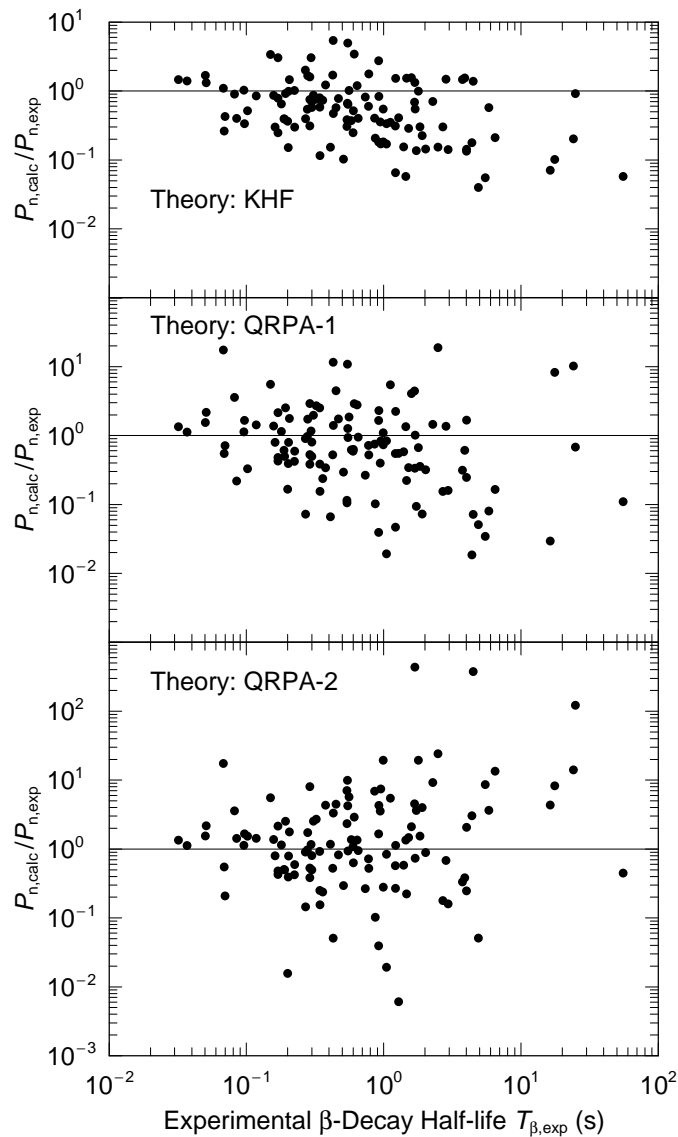


Figure 9: Ratio of calculated to experimental  $\beta$ -delayed neutron-emission probabilities for nuclei in the fission-product region in three different models.

visual inspection of Figs. 8 and 9. As functions of  $T_{\beta,\text{exp}}$  one would expect the average error to increase as  $T_{\beta,\text{exp}}$  increases. This is indeed the case. In addition one is left with the impression that the errors in our calculation are fairly large. However, this is partly a fallacy, since for small errors there are many more points than for large errors. This is not clearly seen in the figures, since for small errors many points are superimposed on one another. To obtain a more exact understanding of the error in the calculation we therefore perform a more detailed analysis.

One often analyzes the error in a calculation by studying a root-mean-square deviation, which in this case would be

$$\sigma_{\text{rms}}^2 = \frac{1}{n} \sum_{i=1}^n (T_{\beta,\text{exp}} - T_{\beta,\text{calc}})^2 \quad (16)$$

Table 5: Analysis of the discrepancy between calculated and measured  $\beta^-$ -decay half-lives shown in Fig. 8.

Model	$n$	$M_{r_1}$	$M_{r_1}^{10}$	$\sigma_{r_1}$	$\sigma_{r_1}^{10}$	$T_{\beta,\text{exp}}^{\text{max}}$ (s)
KHF	115	-0.11	0.77	0.33	2.15	1
QRPA-1	115	-0.02	0.95	0.50	3.14	1
QRPA-2	115	0.13	1.37	0.61	4.04	1
KHF	187	-0.40	0.58	0.41	2.56	all
QRPA-1	187	-0.06	0.87	0.59	3.88	all
QRPA-2	187	0.22	1.67	0.75	5.75	all

However, such an error analysis is unsuitable here, for two reasons. First, the quantities studied vary by many orders of magnitude. Second, the calculated and measured quantities may *differ* by orders of magnitude. We therefore study the quantity  $\log(T_{\beta,\text{calc}}/T_{\beta,\text{exp}})$ , which is plotted in Fig. 8, instead of  $(T_{\beta,\text{exp}} - T_{\beta,\text{calc}})^2$ . We present the formalism here for the half-life, but the formalism is also used to study the error of our calculated  $P_n$  values.

To facilitate the interpretation of the error plots we consider two hypothetical cases. As the first example, suppose that all the points were grouped on the line  $T_{\beta,\text{calc}}/T_{\beta,\text{exp}} = 10$ . It is immediately clear that an error of this type could be entirely removed by introducing a renormalization factor, which is a common practice in the calculation of  $\beta$ -decay half-lives. We shall see below that in our model the half-lives corresponding to our calculated strength functions have about zero average deviation from the calculated half-lives, so no renormalization factor is necessary.

In another extreme, suppose half the points were located on the line  $T_{\beta,\text{calc}}/T_{\beta,\text{exp}} =$

Table 6: Analysis of the discrepancy between calculated and measured  $\beta$ -delayed neutron-emission probabilities  $P_n$  values shown in Fig. 9.

Model	$n$	$M_{r_1}$	$M_{r_1}^{10}$	$\sigma_{r_1}$	$\sigma_{r_1}^{10}$	$P_{n,\text{exp}}^{\text{min}}$ (%)
KHF	86	-0.31	0.49	0.36	2.31	1
QRPA-1	86	-0.12	0.76	0.60	4.02	1
QRPA-2	86	0.12	1.34	0.65	4.51	1
KHF	118	-0.29	0.51	0.44	2.76	all
QRPA-1	118	-0.18	0.66	0.62	4.14	all
QRPA-2	118	0.11	1.28	0.75	5.62	all

10 and the other half on the line  $T_{\beta,\text{calc}}/T_{\beta,\text{exp}} = 0.1$ . In this case the average of  $\log(T_{\beta,\text{calc}}/T_{\beta,\text{exp}})$  would be zero. We are therefore led to the conclusion that there are two types of errors that are of interest to study, namely the average position of the points in Fig. 8, which is just the average of the quantity  $\log(T_{\beta,\text{calc}}/T_{\beta,\text{exp}})$ , and the spread of the points around this average. To analyze the error along these ideas, we introduce the quantities

$$\begin{aligned}
 r &= T_{\beta,\text{calc}}/T_{\beta,\text{exp}} \\
 r_1 &= \log_{10}(r) \\
 M_{r_1} &= \frac{1}{n} \sum_{i=1}^n r_1^i \\
 M_{r_1}^{10} &= 10^{M_{r_1}} \\
 \sigma_{r_1} &= \left[ \frac{1}{n} \sum_{i=1}^n (r_1^i - M_{r_1})^2 \right]^{1/2} \\
 \sigma_{r_1}^{10} &= 10^{\sigma_{r_1}}
 \end{aligned} \tag{17}$$

where  $M_{r_1}$  is the average position of the points and  $\sigma_{r_1}$  is the spread around this average. The spread  $\sigma_{r_1}$  can be expected to be related to uncertainties in the positions of the levels in the underlying single-particle model. The use of a logarithm in the definition of  $r_1$  implies that these two quantities correspond directly to distances as seen by the eye in Figs. 8–9, in units where one order of magnitude is 1. After the error analysis has been carried out we want to discuss its result in terms like “on the average the calculated half-lives are ‘a factor of two’ too long.” To be able to do this we must convert back from the logarithmic scale. Thus, we realize that the quantities  $M_{r_1}^{10}$  and  $\sigma_{r_1}^{10}$  are conversions back to “factor of” units of the quantities  $M_{r_1}$  and  $\sigma_{r_1}$ , which are expressed in distance or logarithmic units.

## DISCUSSION AND SUMMARY

In Tables 5 and 6 we show the results of an evaluation of the quantities in Eq. (17) for  $T_{1/2}$  and  $P_n$  corresponding to  $\beta$  decay of the nuclei in table 1. In the QRPA calculations the ratio between calculated and measured decay half-lives is close to 1.0. This shows, as pointed out earlier (Möller and Randrup, 1990) that *no* renormalization of the calculated strength is necessary. The mean deviation between calculated and experimental half-lives is a factor of 2–5 depending on model and half-life cutoff. Also the calculated  $P_n$  values agree on the average with the experimental data. Here the mean deviation between calculated and experimental data is a factor of 3–6, again depending on model and half-life cutoff. All half-life calculations agree better with data for shorter half-lives, cf. Fig. 8 and Table 5. Therefore one can expect the models to perform better far from stability than what is indicated by the table. The  $\beta$ -delayed neutron emission rates are also better calculated in the region of short half-lives and high  $P_n$  values, cf. Fig. 9 and Table 6. Again, this suggests calculated  $P_n$  values are more reliable far from stability than indicated by Table 6.

The KHF results appear more reliable than the QRPA results. This may seem surprising at first, because the KHF has minimal microscopic content compared to the QRPA. However, an advantage of the QRPA is that it provides so much more detail about  $\beta$ -decay than does the KHF, namely the  $ft$  values of the individual decays, and the transition energies associated with those decays. A very detailed discussion of the possible sources of discrepancies between our QRPA results and experimental data is presented in Ref. (Möller and Randrup, 1990). One difficulty the calculations face is that the calculated half-lives depend on the energy of the transitions as  $(Q_\beta - E)^5$ . As an example we note that calculated half-lives for  $^{95}\text{Rb}$ , for which  $Q_\beta = 9.28$  MeV, change by a factor 1.5 for a change in transition energies by only 0.4 MeV. It is very difficult to reproduce transition energies to this accuracy in a global nuclear-structure model.

For the QRPA-2 calculation we observe that the average of  $T_{\beta,\text{calc}}/T_{\beta,\text{exp}}$  is considerably larger than 1, which corresponds to a correct average. One would have *a priori* assumed that this calculation would be in better agreement with experiment since we substitute *calculated* deformations for spherical deformations when so indicated by experimental data. However, since we do not include  $\beta$ -strength due to forbidden transitions in our model, one would indeed expect that calculated half-lives be too low on the average. The non-spherical deformations that occur, contrary to experimental observations, in the QRPA-1 calculations in some sense simulate the missing low-lying forbidden  $\beta$ -strength. However, a much more satisfying description would be to use correct ground-state deformations and develop some model to account for the strength related to forbidden transitions.

The  $P_n$  values calculated in the QRPA-1 are on the average too low. At present we have no clear explanation for this result. An obvious correction to the model is to take competition with  $\gamma$  emission into account, in particular for emission of  $l_n \geq 3$  neutrons. However, such a correction would further lower the ratio  $T_{n,\text{calc}}/T_{n,\text{exp}}$ . One may speculate that an accounting for *both* this effect and forbidden transition strength in QRPA-2 would bring about satisfactory agreement. This possibility need to be investigated.

We feel strongly that in a global, unified nuclear-structure model a single set of constants must be used over the entire chart of the nuclides, otherwise the basic foundation of the model is violated. However, for the purpose of generating the best possible data bases of half-lives and  $\beta$ -delayed neutron-emission probabilities a complementary approach is reasonable. Just as we feel it is appropriate to use experimental ground-state deformations, experimental single-particle levels, when known, could also be used as the starting point for the QRPA calculations. In practice the situation would be that in some regions, such as near the doubly magic  $^{132}\text{Sn}$ , many half-lives and  $P_n$  values would be unknown, but considerable information on single-particle level order and energies would be available. This experimental information could then be taken into account by locally adjusting the single-particle model proton and neutron spin-orbit strengths and the diffuseness of the single-particle well to obtain optimum agreement with the observed single-particle data such as the observed neutron single-particle sequence  $f_{7/2}$ ,  $p_{3/2}$ ,  $p_{1/2}$ , and  $h_{9/2}$  near  $^{132}\text{Sn}$ . The hope would be that the local agreement would be retained in some limited extrapolation away from the known region. Such a fairly limited extrapolation would be all that is required to reach the

isotopes in the fission-product region where experimental data are not yet available, cf. Fig. 1. Limited studies along these lines have been undertaken by, for example, Hannawald *et al.* (2000). Other highly desirable enhancements to the calculations would be to include first-forbidden strength, perhaps first in a gross-theory approach and later from a new microscopic model. The cut-off parameter  $C$  in the KHF formula could be taken from the Lipkin-Nogami microscopic calculation instead of from the Madland-Nix macroscopic expression. The energy window ( $Q_\beta - S_n$ ) could be reduced by 150 to max 500 keV to account for the angular-momentum barrier for emission of  $l \geq 3$  neutrons in for example  $^{137}\text{I}$ .

In conclusion we note that we now have available about 40 new experimental  $T_{1/2}$  and  $P_n$  values in the fission-product region. Data for additional nuclei in this region that are required as input in reactor criticality, astrophysical and other applications are provided from theoretical calculations. The substantial increase in available experimental data since the compilations by Brady (1989) and Rudstam (1993) is expected to have a significant impact on applied calculations.

## REFERENCES

- Aboussir Y. *et al.* (1995). *Atomic Data and Nucl. Data Tables* **61**, 127.  
 Ameil F. *et al.* (1998). *Eur. Phys. J.* **A1**, 275.  
 Audi, G. (1989). "Midstream atomic mass evaluation, private communication, with four revisions"  
 Audi G. and Wapstra A.H. (1995). *Nucl. Phys.* **A595**, 409.  
 Bernas M. *et al.* (1998). *Nucl. Phys.* **A630**, 41c.  
 Böhmer W. (1998). PhD Thesis, Univ. Mainz, unpublished.  
 Borzov I.N. *et al.* (1996). *Z. Phys.* **A335**, 127.  
 Brady M.C. (1989). "Evaluation and Application of Delayed Neutron Precursor Data", LANL Thesis Report LA-11534-T.  
 Brady M.C. and England T.R. (1989). *Nucl. Sci. Eng.* **103**, 129.  
 Dörfler T. *et al.* (1996). *Phys. Rev.* **C54**, 2894.  
 Duke C.L., Hansen P.G., Nielsen O.B. and Rudstam G. (1970). *Nucl. Phys.* **A151**, 609.  
 England T.R. *et al.* (1986). Specialists' Meeting on Delayed Neutron Properties ISBN 070044 0926 7, p.117. Birmingham, Sep. 1986.  
 Fedoseyev V.N. *et al.* (1995). *Z. Physik* **A353**, 9.  
 Franchoo S. *et al.* (1998). *Phys. Rev. Lett.* **81**, 3100.  
 Gove N.B. and Martin M.J. (1971). *Nucl. Data Tables* **10**, 205.  
 Halbleib Sr J.A. and Sorensen R. A. (1967). *Nucl. Phys.* **A98**, 592.  
 Hamamoto I. (1965). *Nucl. Phys.* **62**, 49.  
 Hannawald M. *et al.* (2000). *Phys. Rev.* **C62**, 054301.  
 Hirsch M., Staudt A., Klapdor-Kleingrothaus H.-V. (1992). *Atomic and Nucl. Data Tables* **51**, 244.  
 Hirsch M., Staudt A., Klapdor-Kleingrothaus H.-V. (1996). *Phys. Rev.* **C54**, 2972.  
 Köster U. (2000). PhD Thesis, TU München, unpublished.  
 Korgul A. *et al.* (2000). *Eur. Phys. J.* **A3**, 167.  
 Kratz K.-L. and Herrmann G. (1973). *Z. Physik* **263**, 435.  
 Kratz K.-L. (1984). *Nucl. Phys.* **A417**, 447.

- Kratz K.-L. *et al.* (2000). *AIP Conf. Proc.* **529**, 295.
- Krumlinde J. and Möller P. (1984). *Nucl. Phys.* **A417**, 419.
- Madland D.M. and Nix J.R. (1988). *Nucl. Phys.* **A476**, 1.
- Mach H., Fogelberg B. and Urban W. (2000). priv. comm. and to be published.
- Mann F.M. *et al.* (1984). *Nucl. Sci. Eng.* **87**, 418.
- Mann F.M. (1986). Specialists' Meeting on Delayed Neutron Properties ISBN 070044 0926 7, p.21. Birmingham, September.
- Mehren T. *et al.* (1996). *Phys. Rev. Lett.* **77**, 458.
- Möller P. and Randrup J. (1990). *Nucl. Phys.* **A514**, 1.
- Möller P. *et al.* (1992). *Nucl. Phys.* **A536**, 61.
- Möller P. *et al.* (1995). *Atomic Data and Nucl. Data Tables* **59**, 185.
- Möller P., Nix J.R. and Kratz K.-L. (1997). *Atomic Data and Nucl. Data Tables* **66**, 131.
- Mueller W.F. *et al.* (2000). *Phys. Rev.* **C61**, 054308.
- Preston M.A. (1962). "Physics of the Nucleus", Addison-Wesley, Reading.
- Pfeiffer B., Kratz K.-L., Möller P. (2000). "Predictions of  $T_{1/2}$  and  $P_n$  Values"; Internal Report, Inst. für Kernchemie, Univ. Mainz (2000).  
URL: [www.kernchemie.uni-mainz.de/~pfeiffer/khf/](http://www.kernchemie.uni-mainz.de/~pfeiffer/khf/)
- Rudstam G. (1993). *Atomic Data and Nucl. Data Tables* **53**, 1.
- deShalit A. and Feshbach H. (1974). "Theoretical Nuclear Physics, vol. I: Nuclear Structure", Wiley, New York
- Shergur J. (2000). Proc. Conf. on *Nuclear Structure 2000 - NS2000*, MSU August 2000; *Nucl. Phys. A*, in print.
- Sorlin O. *et al.* (1993). *Phys.Rev.* **C47**, 2941.
- Sorlin O. *et al.* (2000). *Nucl. Phys.* **A669**, 351.
- Tachibana T., Nakata H., Yamada M. (1998). *AIP Conf. Proc.* **425**, 495.
- Takahashi K. (1972). *Prog. Theoret. Phys.* **47**, 1500.
- Takahashi K. *et al.* (1973). *Atomic Data and Nucl. Data Tables* **12**, 101.
- Wang J.C. *et al.* (1999). *Phys. Lett.* **B454**, 1.
- Weissman L. *et al.* (1999). *Phys. Rev.* **C59**, 2004.
- Wilson W.B. and England T.R. (1993). *Prog. Nucl. Energy*, this volume.